Characterizing structural and lithologic controls on deep-seated landsliding: Implications for topographic relief and landscape evolution in the Oregon Coast Range, USA

Joshua J. Roering[†]
Department of Geological Sciences, University of Oregon, Eugene, Oregon 97403-1272, USA

James W. Kirchner
William E. Dietrich
Department of Earth and Planetary Science, 307 McCone Hall, University of California, Berkeley, California 94720-4767, USA

ABSTRACT

In mountainous areas, landslides regulate temporal variations in sediment production and may suppress simple linkages between topographic development and tectonic forcing. Rates and mechanisms of mass wasting depend on lithology, bedrock structure, and climatic and tectonic setting. These factors tend to vary significantly in active tectonic regions, thus clouding our ability to predict how landsliding modulates topographic development over human and geological time scales.

Here, we use a novel DEM-based technique to document the distribution of large landslides in the Oregon Coast Range (OCR) and quantify how they affect topographic relief. We developed an automated algorithm that exploits the distinctive topographic signature (specifically the relationship between curvature and gradient) of large landslides to map their distribution within the gently folded Tyee Formation (Eocene deltaic-submarine ramp sediments). In contrast to steep and highly dissected terrain frequently identified as characteristic of the OCR (which exhibits steep, planar side slopes and highly curved, low-gradient ridge tops and valleys), terrain prone to large landslides tends to have low values of both drainage density and curvature and gradient values that cluster between 0.16 and 0.44. The distribution of failure-dominated terrain in our 10,000 km^2 study area is influenced by systematic variations in sedimentary facies and bedrock structure. The fraction of terrain altered by large landslides (>0.1 km^2) varies from 5% in the sand-rich (delta-slope and proximal ramp facies) southern section of our study area to ~25% in the north (distal ramp facies), coincident with an increase in the thickness of siltstone beds and a decrease in the sandstone:siltstone ratio. Local relief declines progressively northward, suggesting that deep-seated landsliding is sensitive to the thickness and frequency of low-shear-strength siltstone beds and may serve to limit topographic development in the OCR. Structural controls are superimposed on facies-related variations as deep-seated landslides are frequently found on slopes whose downslope aspect corresponds to the bedrock dip direction. For 1516 strike and dip measurements in our study area, we calculated the fraction of proximal terrain (<2.5 km) altered by deep-seated landsliding. In the sand-rich southern region, the proportion of proximal slide-dominated terrain increases modestly with bedrock dip. In the silt-rich northern region, terrain altered by deep-seated landsliding is pervasive, and an increase in dip from 0° to 16° corresponds to a change in the fraction of slide-prone terrain from 10% to 28%.

Our technique for mapping large landslides has utility for hazard analysis and land management. Over million-year time scales, the progradational character of the Tyee Formation suggests that continued uplift and exhumation of the OCR should result in a southward propagation of slide-prone, silt-rich distal facies. As a result, deep-seated landsliding will become increasingly prominent, and topographic relief in the central and southern OCR will progressively decline. Whereas spatial variability in climatic or tectonic forcing is often invoked to explain systematic variations in topographic development, our results emphasize the importance of structural and intraformation lithologic controls on landsliding. As such, analyses linking surface processes, climate, tectonics, and landscapes should be couched in the context of diverse geologic and topographic data.

Keywords: deep-seated landslides, landscape evolution, Oregon Coast Range, slope stability, Tyee Formation, relief.

INTRODUCTION

The morphology of mountainous terrain reflects the complex interplay of tectonic, climatic, and erosional processes. Given that most mountainous landscapes are characterized by significant variations in lithology, climate, rock uplift rate, and surficial processes, earth scientists face a daunting task in isolating how these factors affect landscape properties such as relief and average gradient. Since the pioneering work of Ahnert (1970), relief has been used as a proxy for tectonic forcing, and with the advent of digital elevation modeling, it can be easily assessed over broad areas (e.g., Ahnert, 1984; Pinet and Souriau, 1988; Ohmori, 1993; Summerfield and Nulton, 1994; Hurtrez et al., 1999; Montgomery et al., 2001; Willett et al., 2001; Gabet et al., 2004). The hypothesis that climate-driven shifts in rates and mechanisms of valley incision can increase relief (Molnar and England, 1990; Zhang et al., 2001) highlights the importance of understanding how relief is regulated through feedbacks between erosional processes and tectonic forcing. Although it was originally hypothesized that relief primarily reflects the interaction between rock uplift and valley-forming fluvial processes or glacial incision (Ahnert, 1970; Whipple et al., 1999; Brocklehurst and Whipple, 2002; Hooke, 2003; Roe et al., 2003), many studies suggest that relief may be limited by mass wasting processes (Carson and Petley, 1970; Schmidt and Montgomery, 1995; Kuhni

[†]E-mail: jroering@uoregon.edu.

GSA Bulletin; May/June 2005; v. 117; no. 5/6; p. 654–668; doi: 10.1130/B25567.1; 12 figures; 1 table.

and Pfiffner, 2001; Roering et al., 2001; Montgomery and Brandon, 2002; Lague and Davy, 2003; Stock and Dietrich, 2003), such that tectonic forcing and relief may be effectively decoupled. The notion that bedrock landsliding, in particular, can fundamentally alter landscape characteristics at the orogen scale by truncating hilltops, inhibiting valley incision, or manipulating drainage divides is intuitively appealing, although difficult to demonstrate. The nature of mass wasting processes varies significantly among landscapes, and such variation likely precludes a global relationship that governs relief-limiting conditions.

The occurrence and activity of deep-seated landslides (defined here as bedrock landslides that have a surface area >0.1 km^2, incorporate predominantly parent material in the slide mass, and do not run out long distances) reflect a variety of environmental and geologic factors (e.g., Schuster, 1978; Palmquist and Bible, 1980; Miller and Sias, 1998). In general, deep-seated landslides result from a combination of long-term factors that condition slopes for failure (such as channel incision, slope morphology, geologic structure, shear strength loss due to weathering, and lithologic variation) and short-term processes that tend to trigger instability (such as hydrologic and seismic events). Whereas large landslides have been shown to respond to mining and dam building (e.g., Voight, 1978), their sensitivity to timber harvesting, road building, and changes in surface hydrology are currently debated (de la Fuente et al., 2002; Gerstel and Badger, 2002). Owing to their substantial volume, deep-seated landslides have a long-lived morphologic legacy (e.g., Wieczorek, 1984; Densmore et al., 1998; Hovius et al., 1998; Densmore and Hovius, 2000; Mather et al., 2003). As a result, the observed distribution of bedrock landslides across a particular landscape reflects both spatial variability in conditions that contribute to slope instability and variation in the time since slope failure occurred. Although several studies have characterized landslides in relation to a particular tectonic and climatic setting (Hermanns and Strecker, 1999; Trauth and Strecker, 1999; Hermanns et al., 2000; Trauth et al., 2000; Pratt et al., 2002; Gabet et al., 2004), most field-based analyses that decipher spatial and temporal patterns of bedrock landsliding are limited in scope because methods available to identify slope instability (including aerial photo mapping and remote sensing analyses) are laborious and subjective (van Asch and van Steijn, 1991; Cendrero and Dramis, 1993; Hovius et al., 1997; Larsen and Torres-Sanchez, 1998; Shroder, 1998; Dikau and Schrott, 1999; Gonzalez-Diez et al., 1999). Recent statistical analyses have successfully quantified the size distributions of landslides for determining the geomorphic significance of landslide size classes and assessing hazards (e.g., Harp and Jibson, 1996; Hovius et al., 2000; Stark and Hovius, 2001; Malamud et al., 2004); however, such approaches do not address how landslides are distributed in relation to other landscape characteristics. As a result, we lack the ability to decipher how large landslides respond to tectonic and climatic forcing and regulate topographic development.

Over the last several decades, the Oregon Coast Range (OCR) has proven to be a fruitful study area for analyzing sediment production and transport processes because rates of erosion and tectonic forcing are relatively well constrained and the region did not experience Pleistocene glaciation (Reneau and Dietrich, 1991; Personius, 1995; Kelsey et al., 1996; Roering et al., 1999; Heimsath et al., 2001). Although most mass wasting studies in the OCR have focused on quantifying shallow landsliding and debris flow erosion and their effect on landscape function over human and geologic time scales (Dietrich and Dunne, 1978; Benda, 1990; Reneau and Dietrich, 1990; Montgomery et al., 2000; Schmidt et al., 2001; May, 2002; Lancaster and Hayes, 2003; May and Gresswell, 2003; Stock and Dietrich, 2003), numerous landslide-dam lakes in the OCR suggest that deep-seated landslides may also play a role in shaping the region (Baldwin, 1958; Lane, 1987). The low-gradient, benchlike morphology of these large, bedrock landslides is distinctive from the steep and dissected nature of debris-flow–prone terrain that is often cited as characteristic of the OCR. Few of these deep-seated slides have exhibited historical activity, as most are characterized by degraded headscarps and poorly defined margins. The timing of these slope failures is poorly constrained, but the large extents (~2–4 km) of alluvial fills upstream of several landslide-dam lakes (Baldwin, 1958) suggest that such failures may have a significant and persistent influence on landscape morphology and temporal patterns in sediment yield.

In this contribution, we describe a novel methodology for delineating the spatial distribution of deep-seated landslides that enables us to document and predict their role in the evolution of the OCR. The goals of this study are to: (1) formulate and test an automated algorithm that uses digital topographic data to identify the extent of terrain affected by deep-seated landsliding, (2) illustrate and quantify how geological structure and lithology control the spatial distribution of slope instability, and (3) use geologic constraints to interpret and predict how large landslides evolve in response to rock uplift and affect topographic relief over million-year time scales. Our approach contrasts with site-specific slope stability analyses in that the details of individual landslides are jettisoned in favor of a coarse regional assessment of landslide frequency. Our current understanding of how rock uplift modulates topographic form and relief in the OCR has been focused on quantifying the relative efficacy of fluvial and debris flow incision via analysis of channel networks (Seidl and Dietrich, 1992; Sklar and Dietrich, 1999; Stock and Dietrich, 2003). The presence of large landslides in this area, however, motivates us to ask several questions. Is it possible that deep-seated landsliding imparts a first-order control on landscape development, locally obscuring simple relationships that link tectonic forcing with channel network metrics? If so, how will lithologic and structural variations dictate the spatial pattern of large landslides and local relief with continued rock exhumation? The analysis described here emphasizes the importance of coupling sedimentology, stratigraphy, bedrock structure, neotectonic, and climatic data sets to quantify how surface processes modulate landscape evolution.

STUDY AREA

The Oregon Coast Range is a humid, soil-mantled landscape largely composed of Eocene sedimentary rocks that overlie volcanic basement accreted to the North American plate in the early Tertiary (Orr et al., 1992). Locally, basaltic dikes crop out within the Tyee Formation and tend to form prominent peaks (Walker and MacLeod, 1991). We developed our algorithm to identify deep-seated landslides occurring in Eocene sedimentary rocks, specifically the Tyee Formation, which is a sand-rich, delta-fed turbidite system (Heller and Dickinson, 1985) that covers a large portion of the central OCR (Fig. 1).

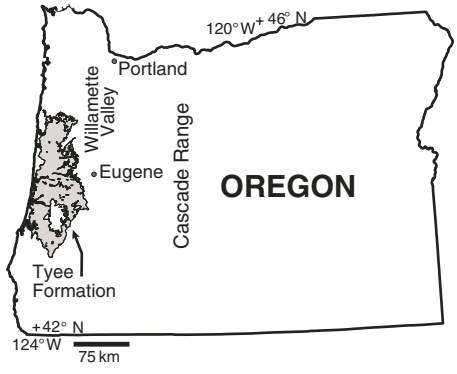

Figure 1. Location map of the Tyee Formation (Eocene sedimentary rocks) in the central Oregon Coast Range.

The depositional setting of the Tyee Formation has been studied in detail because of its distinct assemblage of sedimentary facies (Lovell, 1969; Chan and Dott, 1983; Heller and Dickinson, 1985). Heller and Dickinson (1985) suggested that a sand-rich sequence of turbidite deposits that constitutes much of the Tyee Formation originated from a delta-fed submarine ramp depositional system. Sedimentologic properties within the early Eocene sedimentary system vary primarily with latitude, as the underlying crustal block has been rotated clockwise 40°–70° due to oblique subduction along the Pacific Northwest margin of North America (Heller and Ryberg, 1983). In contrast to more classical interpretations of submarine canyon systems (Mutti and Ricci-Lucchi, 1978), no single channel served as a discrete point source for the turbidite beds of the Tyee Formation. Instead, a series of channels developed along the base of the continental slope and conveyed sediment into the basin, such that lateral (east-west) facies variability within the Tyee Formation is minimal (Heller and Dickinson, 1985). North-south–oriented facies changes, which are characterized by depositional structures, bed thickness, and the sandstone:siltstone ratio, are the dominant source of lithologic variation within the Tyee Formation (Chan and Dott, 1986). In the south, deltaic and shallow continental shelf deposits have a high percentage of sandstone (>90%), cross-bedding, and thick (>3 m) beds. Moving north, bed thickness and the sandstone:siltstone ratio decrease as slope and proximal ramp sediments grade into distal ramp and ramp fringe sediments (Chan and Dott, 1983; Heller and Dickinson, 1985). The stratigraphic succession described by Chan and Dott (1983) indicates a general shoaling in the northward direction and a progradation of facies across the basin. Situated in the southern half of our study area, a large patch of highly indurated, late Eocene sediments of the Elkton Formation (which are younger than the Tyee Formation) occurs and tends to form steep bedrock cliffs that contrast with topography associated with the Tyee Formation (Fig. 2A). By confining our analyses to the Tyee Formation, we isolate the influence of bedrock structure and facies-related lithologic variations on deep-seated landsliding and topographic development.

Since the late Eocene, the Tyee Formation has been compressed into a series of low-amplitude, gently dipping folds (the maximum dip of bedding along the flanks of folds rarely exceeds 15°–20°) oriented NNE (Fig. 2A) (Baldwin, 1956). Uplift of the OCR commenced in the Miocene (McNeill et al., 2000) and continues today as evidenced by abandoned wave-cut platforms along the Oregon coast (Kelsey et al., 1996). Rates of rock uplift derived via dating of marine terraces adjacent to our study area (latitude ranging from 43°–45°) vary from 0.1–0.3 mm yr^{-1} (Kelsey et al., 1996) and are generally an order of magnitude lower than geodetic uplift rates derived from highway leveling and tide gauge data (Mitchell et al., 1994). Both short- and long-term uplift rates measured along the coast vary locally due to vertical movement along faults, although it is unclear whether these local variations extend a significant distance inland (Kelsey et al., 1996).

The topography of the OCR has been characterized as steep and highly dissected with relatively uniform ridge and valley terrain (Fig. 3A) (Dietrich and Dunne, 1978; Reneau and Dietrich, 1990, 1991; Montgomery, 2001). Typically, soil (defined here as the mobile layer overlying weathered bedrock or saprolite) is relatively thin (~0.5 m) on hilltops and side slopes and thicker (~1–2 m) in unchanneled valleys that act as preferential source areas for shallow landslides that often initiate debris flows (Dietrich and Dunne, 1978; Montgomery and Dietrich, 1994; Heimsath et al., 2001). Most studies of decadal-to-millenial scale patterns of sediment production and delivery in the OCR have focused on the cyclic infilling and evacuation of soil in steep, convergent areas (Dietrich et al., 1982; Reneau and Dietrich, 1991; Benda and Dunne, 1997). Erosion rates generated by short-term (~10 yr) and long-term (~5000 yr) analyses of sediment yield are commonly 0.05–0.3 mm yr^{-1} (Beschta, 1978; Reneau and Dietrich, 1991; Heimsath et al., 2001), consistent with rates of coastal uplift (Kelsey et al., 1996) and Holocene bedrock channel incision (Personius, 1995). These studies have been used to argue that an approximate balance exists between rock uplift and erosion in the OCR such that the topographic form may be relatively uniform with time (Reneau and Dietrich, 1991; Roering et al., 1999; Montgomery, 2001). Short, steep hillslopes that erode via nonlinear slope-dependent processes can rapidly (~40 k.y.) adjust their morphology to climatic or tectonic perturbations (Roering et al., 2001), enabling a tendency toward steady-state erosion. In contrast, deep-seated landslides produce topographic features that persist for 10–100 k.y., and temporal patterns of sediment production associated with these large failures are unconstrained.

PREVIOUS STUDIES OF DEEP-SEATED LANDSLIDING IN THE OREGON COAST RANGE

Noting the preponderance of landslide-dam lakes (Table 1), Baldwin (1958) suggested that steep, incised valleys of the OCR tend to promote large-scale (10^5–10^9 m^3) slope failures resulting from precipitation or seismic events. Landslides documented by Baldwin (1958) exhibited hummocky topography with small, undrained depressions (Fig. 3B). Chronological evidence for the timing of landsliding is sparse. Based on radiocarbon data, the ages of two large lakes, Triangle and Loon, were estimated at >40,000 and 1400 yr, respectively (Baldwin, 1958; Worona and Whitlock, 1995). Only a handful of these landslides have experienced historical movement, although the degree of slope movement and morphologic alteration is variable. In the winter of 1955–1956, Camp Creek (just north of the Umpqua River near the northern extent of the Elkton Formation, Fig. 2) was dammed by an active landslide and formed a temporary lake that breached within the year (Baldwin, 1958). On December 6, 1975, an ~400-m-long segment of Drift Creek (located in the Alsea River catchment) was inundated with landslide material tens of meters thick. The landslide formed an ~60-m-high headscarp near the ridge top and traveled ~400 m downslope (Thrall et al., 1980). This event, termed the Drift Creek slide, reactivated a fossil landslide deposit following a week of heavy rain. Ayers Lake formed rapidly behind the landslide dam and persists today. Timber harvesting and road construction were active on the slope in the months prior to failure, but their impact on the instability is uncertain. In the winter of 1998–1999, Steinhauer Creek (a tributary

Figure 2. Elevation and deep-seated landslide terrain in the Tyee Formation. (A) Elevation with mapped distribution of anticlines and synclines (Baldwin, 1956, 1959, 1961). (B) Distribution of β values that quantify the degree to which terrain exhibits the topographic signature of deep-seated landsliding (see text). β varies from 0 to 1; 0 corresponds to steep and dissected terrain without indication of deep-seated landsliding and 1 represents terrain with morphology consistent with that generated by deep-seated landslides. On the basis of field observations and air photo analysis, β = 0.33 (which corresponds to the transition from burnt yellow to red) suitably demarcates boundaries of slide masses. In the southern interior, a patch of highly indurated, late Eocene sediments of the Elkton Formation occurs and tends to form steep bedrock cliffs that contrast with the topography of the Tyee units.

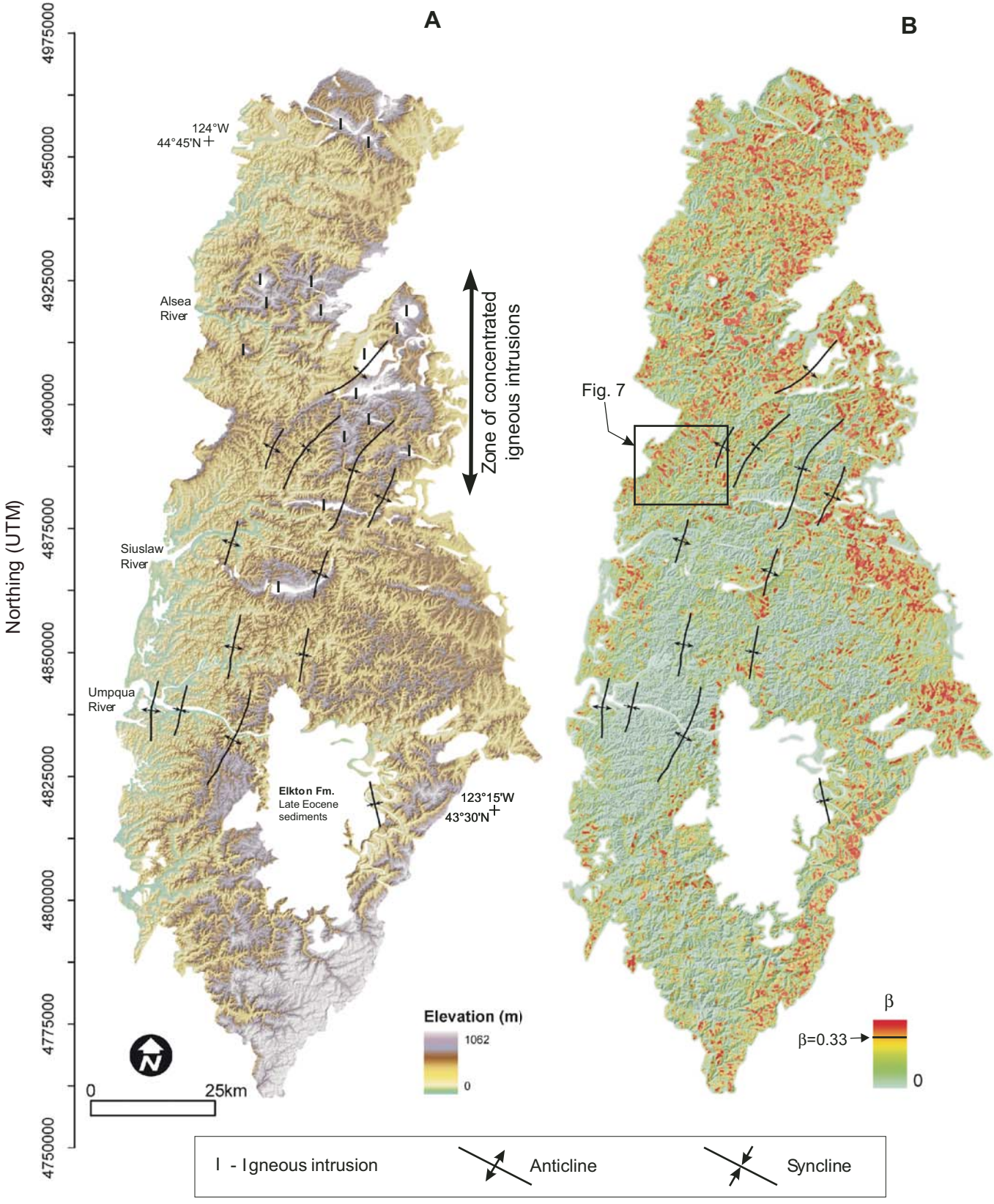
A
B
Northing (UTM)
4975000
4950000
4925000
4900000
4875000
4850000
4825000
4800000
4775000
4750000
124°W
44°45'N
Alsea River
Siuslaw River
Umpqua River
Zone of concentrated igneous intrusions
Fig. 7
Elkton Fm.
Late Eocene sediments
123°15'W
43°30'N
Elevation (m)
1062
0
β
β=0.33
0
0
25km
I - Igneous intrusion
Anticline
Syncline

of Siuslaw River) was inundated by sediment from a deep-seated landslide that left a 30-m-high headscarp. Slow, continuous deformation continued through the season and in subsequent winters (Seward, 1998, personal commun.). Other historical landslides have exhibited brief periods of slow movement (<1 m yr^{-1}) that followed periods of heavy rainfall but did not fail catastrophically (Wong, 1991).

Lane (1987) noted a correspondence between the downslope aspect of four lake-forming landslides and the dip direction of the local bedrock and suggested that the slide failures may be localized along the sandstone-siltstone interfaces of the Tyee Formation (Fig. 4). Despite the historical activity of the slides discussed above, most of the slumplike terrain in the OCR (as described by Baldwin, 1958) appears dormant. In contrast to steep and dissected regions, soil profiles observed in roadcuts on these ancient landslides tend to be very thick (>2–3 m), dense, and highly weathered (Roering et al., 1996). Areas of pervasive deep-seated landsliding in the OCR may represent a significant departure from erosional equilibrium relative to the time scale of soil transport and shallow landsliding (~10^4 yr) that dictates the evolution of steep and dissected terrain in the OCR. More generally, the role of deep-seated landsliding in regulating sediment production and landscape morphology is poorly understood.

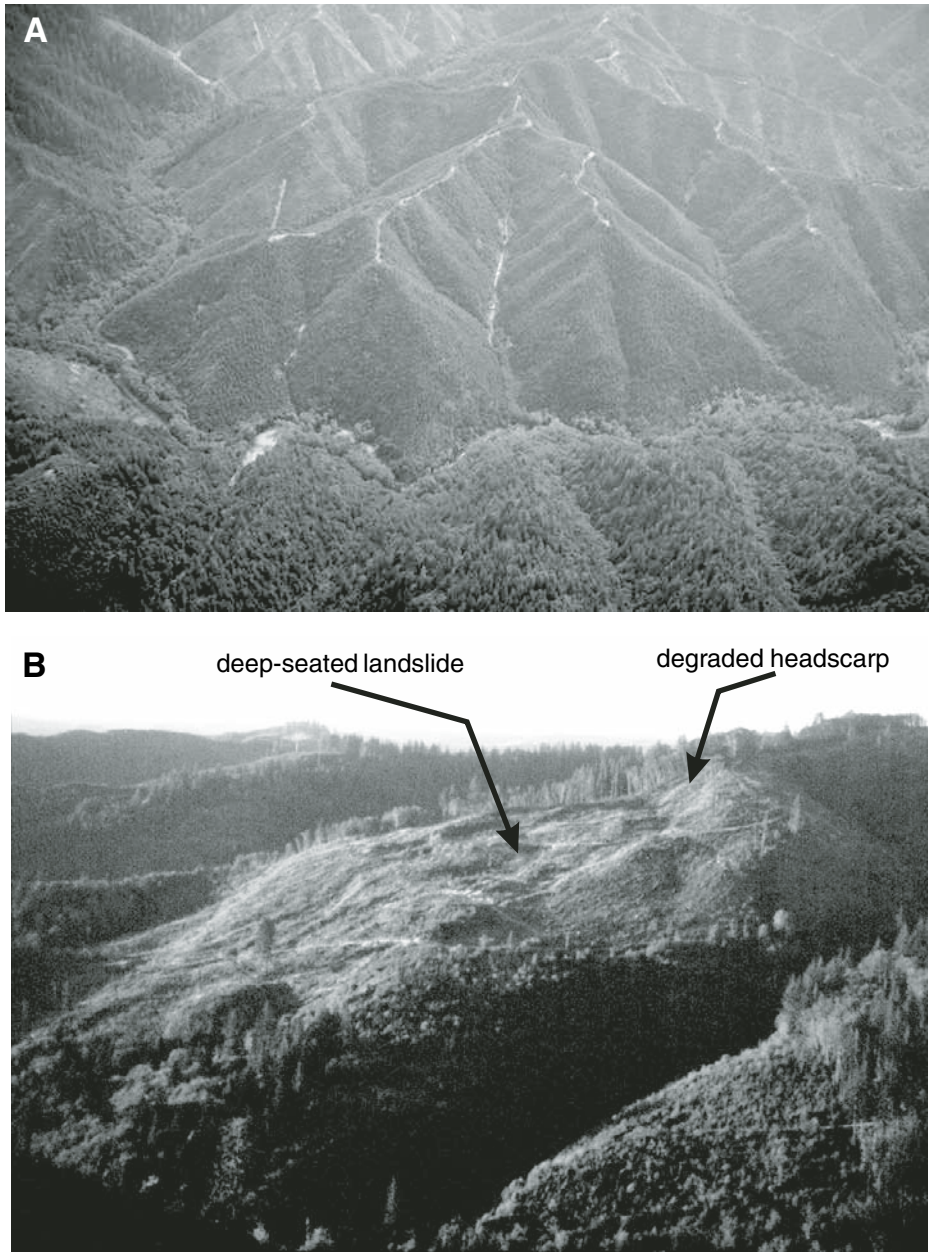

Figure 3. Oblique photos of (A) steep and dissected terrain often cited as characteristic of the Oregon Coast Range (OCR), and (B) an ancient deep-seated landslide in the OCR (latitude: 43.47°N, longitude: 124.12°W) that exhibits a low-gradient, benchlike morphology.

TOPOGRAPHIC IDENTIFICATION AND MAPPING OF DEEP-SEATED LANDSLIDES

Here, we exploit the profound morphologic manifestation of deep-seated landslides in the OCR to automatically map their extent using a digital elevation model (DEM). Figure 5 illustrates an east-west–trending ridge line with characteristic forms on either side; the north-facing flank of the ridge is distinguished by steep and dissected terrain, whereas the southern flank exhibits a benchlike, low-gradient form. On the northern side, the integrated valley network facilitates the delivery of sediment from hillslopes and topographic hollows to higher-order channels via debris flows (Dietrich and Dunne, 1978; Benda and Dunne, 1997). In contrast, the poorly dissected slopes on the southern side arise from deep-seated slope instability that occurs frequently enough to suppress the development of valley networks (Fig. 5). No historical deformation has occurred at this site, but degraded headscarps similar to those shown in Figure 3B attest to the history of slope deformation. Along the base of the ancient landslide, valley incision has steepened slopes at the channel margin. Similarly steep sections were commonly observed during our field investigations of over 40 ancient deep-seated landslides in the OCR. Typically, dormant landslides exhibit: (1) >10-m-high, degraded headscarps, (2) low-gradient, hummocky benches with poorly developed drainage, and (3) steep lower slopes with active streamside soil slips. At some sites, the steep, lower slope segment, which may reflect the legacy of valley incision (Kelsey, 1988; Densmore and Hovius, 2000), was poorly developed or absent.

Method

The topographic signature of deep-seated slope failure is immediately apparent via inspection of aerial photos and topographic maps. To streamline the mapping process, we formulated a quantitative method for delineating landslide-dominated terrain from DEM data. For this endeavor, we acquired a DEM of the Oregon Coast Range from the USGS National Elevation Data set (NED), which has a grid spacing

TABLE 1. LANDSLIDE-DAM LAKES IN THE OREGON COAST RANGE

Name	Latitude (N)	Longitude (W)	Chronology
Ancient Lake Sitkum†	43.143°	123.866°	?
Ayers Lake	44.458°	123.785°	Drift Creek slide: Dec. 6, 1975
Bradish Lake	44.605°	123.701°	?
Camp Creek (temporary lake)	43.607°	123.778°	Camp Creek slide: winter, 1956
Esmond Lake	43.871°	123.598°	?
Gould (Elk) Lake	43.535°	123.943°	?
Loon Lake†	43.585°	123.837°	>1400 yr B.P.
Lost Lake	43.285°	123.606°	?
Triangle Lake†	44.172°	123.571°	>42,000 yr B.P.
Wasson Lake	43.747°	123.793°	?
Yellow Lake	43.799°	123.554°	?

†Large lake with upstream alluviated valley greater than 4 km in length (Baldwin, 1958; Thrall et al., 1980; Lane, 1987).

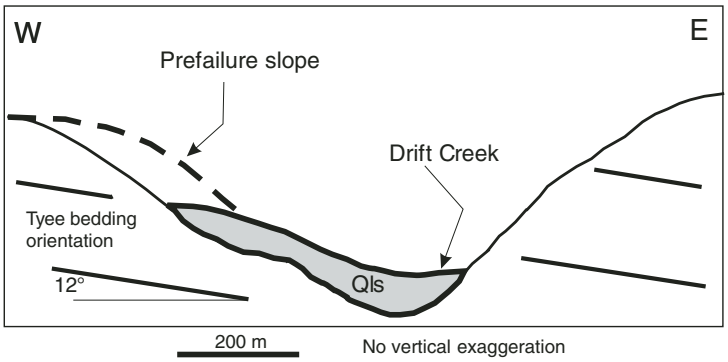

Figure 4. Schematic cross section of Drift Creek landslide (Dec. 6, 1975). Modified after Lane (1987). Qls refers to Quaternary landslide deposit.

of ~26.5 m and boasts minimal edge matching and other artifacts. We compared the data against available 10 m DEMs and concluded that the 26.5 m data set was sufficient for distinguishing the topographic signature of deep-seated landsliding and allowed for faster computational time. Using a digital database derived from the Oregon State geological map (Walker and MacLeod, 1991), we clipped topography from the DEM with a digital coverage outlining the extent of the Tyee Formation (see Fig. 2A). Small voids in the clipped topography (shown with the letter "I" superimposed) represent igneous intrusive rocks that are more resistant to erosion than the Tyee Formation and tend to be associated with large knickpoints in river profiles.

We used topographic maps, aerial photos, and field observations to identify and map several ridges that exhibit both steep and dissected terrain and deep-seated landslide-prone terrain (see Fig. 5). Reasoning that the morphologic differences that distinguish the two process domains may be reflected by their slope and degree of curvature, we calculated the distribution of topographic derivatives gradient ($|\nabla z|$) and curvature (estimated here as the Laplacian operator, $\nabla^2 z$) for both sides of each ridge using algorithms summarized by Zevenbergen and Thorne (1987) and Moore et al. (1991). Positive values of curvature reflect concave terrain such as that associated with unchanneled valleys or hollows, whereas negative values represent convex forms such as hilltops. We plotted the variation of curvature with gradient for steep and dissected terrain, deep-seated landslide terrain, and nearby valley floors (two examples are shown in Fig. 6). With minimal overlap, each landform type exhibits its own morphologic signature in gradient-curvature space. We defined the range of gradient and curvature values that best distinguishes the cluster of points associated with deep-seated landslides. For various combinations of gradient and curvature values, we calculated the fraction of deep-seated, valley floor, and steep/dissected data that fall within the topographic envelope. To determine the best-fit envelope, we simultaneously maximized the fraction of deep-seated data and minimized the fraction of valley floor and steep/dissected data that plot within the topographic envelope. The calibrated morphologic envelope indicates that deep-seated landslides (filled circles on Fig. 6) are distinguished by near-zero values of curvature ($|\nabla^2 z| < 0.008$ m^{-1}) and $|\nabla z|$ values between 0.16 and 0.44 (see gray box in Fig. 6). In contrast, planar regions of the steep and dissected terrain tend to be associated with steep sideslopes ($|\nabla z| > 0.5$) and low-gradient regions (hilltops or narrow valley axes with $|\nabla z| < 0.4$) exhibit highly negative or positive values of $\nabla^2 z$. Wide valley floors were distinguished by near-zero curvature values and gradients uniformly lower than those observed on slide-prone terrain (Fig. 6). For the data sets depicted in Figure 6A and 6B, more than 92% of the deep-seated landslide data fall within our topographic envelope, whereas less than 8% and 4% of the valley floor and steep/dissected data points, respectively, plot within the envelope.

We used spatial averaging in applying the topographic signature of deep-seated landslides to the DEM of our study area. First, we identified every grid node within the DEM having gradient and curvature values that fall within our deep-seated morphologic criteria. The resulting binary grid (values of either 0 or 1, with 1 indicating inclusion in the deep-seated topographic envelope) revealed a speckled pattern in some landslide-dominated areas, as localized zones within individual deep-seated landslides did not fall within the topographic envelope. To account for the spatial scale of individual landslides and de-emphasize local deviations from the morphologic criteria, we smoothed the grid of binary data at each node by calculating the proportion of adjacent terrain that met the topographic criteria. Specifically, we generated another grid whose values were calculated as the fraction of points within a 250 m radius that fell within the deep-seated landslide topographic envelope. Values for the resulting data set, which we term β values, vary continuously from 0 to 1.0, with 0 representing terrain without adjacent landslide-dominated slopes and 1.0 indicating that all of the adjacent terrain exhibits morphology indicative of deep-seated landsliding. For this analysis, we chose a 250 m smoothing radius because it represents the approximate planform dimension of several deep-seated landslides we identified from field surveys and air photo inspection. Larger radii tend to diffuse the signal of individual landslides and smaller radii tend to partition individual landslides into several sections.

Results

Using our automated algorithm, we estimated the distribution of topography indicative of deep-seated slope failure in the Tyee Formation (Fig. 2B). In Figures 2B and 7, high values of β (terrain exhibiting slide-dominated morphology)

are represented with warm colors (yellow, orange, and red) and low values with cool colors (green and light blue). To calibrate the particular value of β that corresponds with the margin of landslide-prone slopes, we examined the distribution of β values at numerous locations where we previously identified deep-seated landslides via aerial photos, field observations, and topographic maps. At these sites, β >0.33 served as an accurate criterion for delineating the boundaries of deep-seated landslides. Strictly interpreted, this indicates that for a given grid point with β = 0.33, 33% of the surrounding patch of terrain has values of gradient and curvature that meet the topographic criteria (Fig. 6). The coarse dashed line on Figure 5 illustrates the region within which values of β exceed 0.33. Although some details (such as steep, inner gorges associated with slope failure along channel margins), may not be precisely resolved, the β >0.33 boundary generally corresponds to the zone of landslide-dominated topography (Fig. 5).

β values in the Tyee Formation vary latitudinally (Fig. 2B). In the southern portion of our study area, β values are generally low but locally variable. Moving north, β values increase progressively such that a large fraction of slopes in the northern portion of our study area exhibits β >0.33 (shown as red in Fig. 2B). Several large zones of high β values also occur along the eastern margin of the Tyee Formation. The central and southwestern regions exhibit low β values as slope morphology is dominated by steep and dissected terrain driven by debris flow initiation and runout.

The spatial extent of our study area (~10,000 km^2) prevented us from verifying a significant portion of the slopes we identified as failure prone. Using field observations, aerial photos, topographic maps, and maps of landslide-dam lakes, we tested the algorithm at over 40 sites and concluded that it consistently separated deep-seated landslides from steep/dissected terrain and valley floors. Locally, the algorithm misidentified fluvial meander slip-off surfaces (i.e., the inner banks of large bedrock meanders) as slide-dominated because they tend to exhibit smooth, low-gradient surfaces (Fig. 7). These features are isolated to isolated zones along major rivers and thus constitute a negligible fraction of the landslide-prone (high β) terrain shown in Figure 2B.

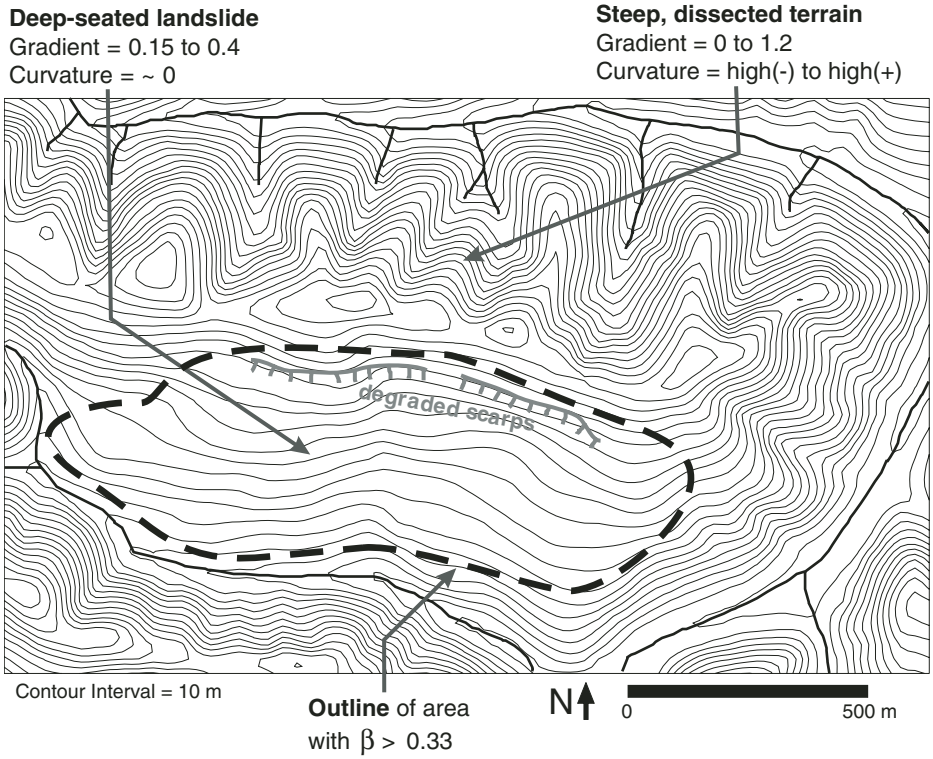

Figure 5. Contour map of a ridge in our study area (latitude: 43.855°N, longitude: 123.541°W) that exhibits steep and dissected terrain on its northern side and an ancient deep-seated landslide on the southern flank. Field observations on the landslide revealed degraded scarps near the ridge crest not distinguishable from topographic data. The thick, dashed line illustrates the outer edge of terrain with β >0.33, which delimits boundaries of deep-seated landslide morphology (see text).

LITHOLOGIC CONTROLS ON LANDSLIDING AND TOPOGRAPHIC RELIEF

Method

To explore how lithologic variations within the Tyee Formation affect the development of landslide-prone terrain, we quantified how β values vary in accordance with latitudinal facies changes. As discussed above, sand-rich deltaic and proximal ramp deposits found in the southern half of the Tyee Formation grade northward into silt-rich distal and ramp fringe deposits. We quantified north-south topographic variations by partitioning our grid of β v alues into a series of horizontal swaths, each measuring 12.5 km in the north-south direction and spanning the study area in the east-west direction. Within each swath, we calculated the fraction of terrain (hereafter referred to as *F*) exhibiting the topographic signature of deep-seated landsliding (i.e., with β >0.33). To investigate the effect of deep-seated landslides on topographic development, we calculated the distribution of local relief at two different spatial scales. For each grid node in our study area, we calculated local relief as the difference between the highest and lowest elevation values within a circular window. We performed separate analyses using a 250 m window to represent relief at the scale of individual ridges and valleys and a 2.5 km window to represent the regional distribution of relief encompassing several nearby ridge/valley sequences (Roering et al., 2001).

Results

Our analysis reveals systematic latitudinal variation in deep-seated landsliding, as β values tend to be relatively low in the south and increase to the north (Fig. 8). This pattern may reflect facies variability within the Tyee Formation (Chan and Dott, 1983; Heller and Dickinson, 1985). In the southern region, landslides comprise 5%–10% of the landscape, whereas for latitudes greater than 44°, the proportion of slide-prone terrain consistently exceeds 15%–20% (Fig. 8A). This relatively discrete transition corresponds with a significant change in the sandstone:siltstone ratio (from 9:1–6:4) and a shift from proximal to distal ramp facies. The overall pattern shown in Figure 8A does not result from variation in structural controls as the orientation of bedrock does not vary systematically with latitude (see below). Instead, the high proportion of slide-dominated

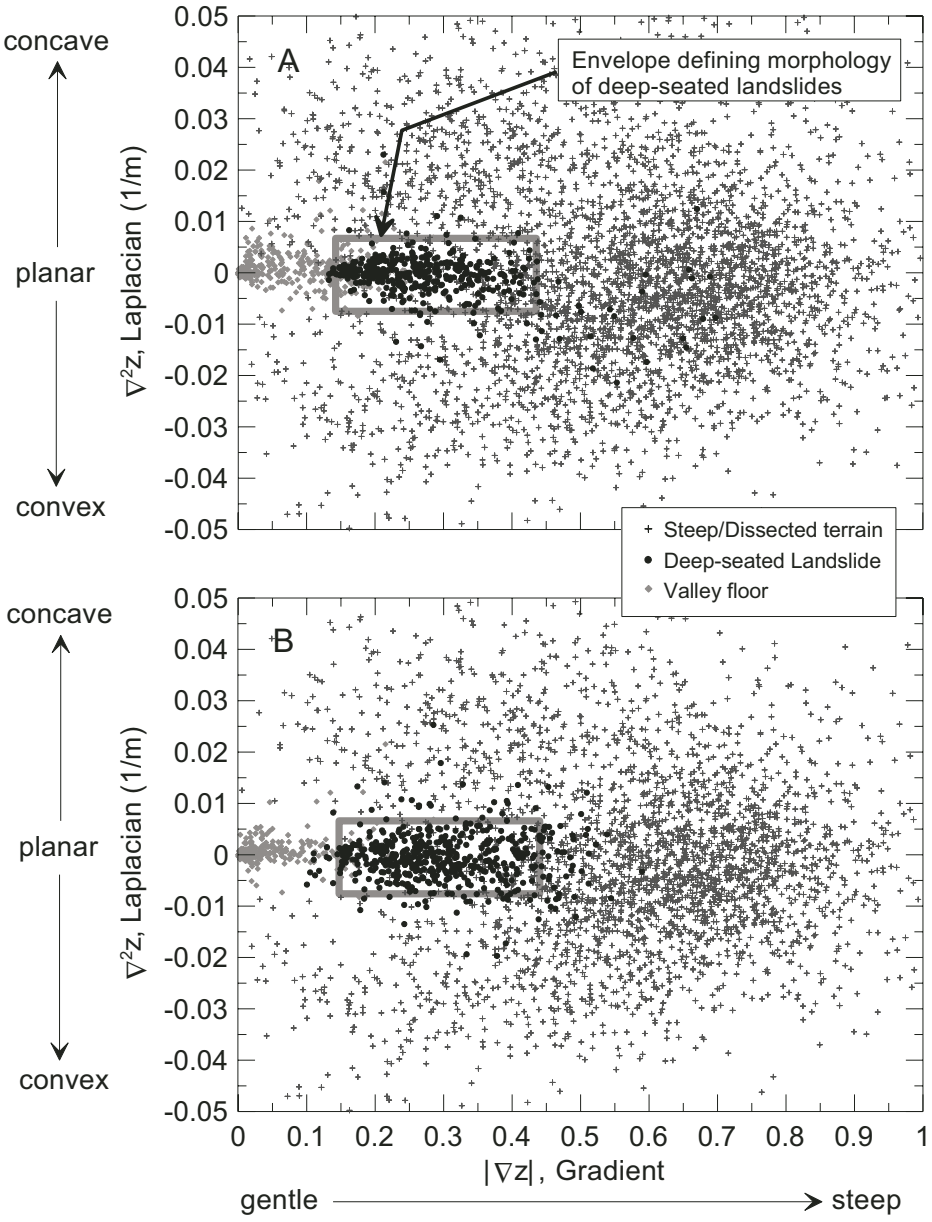

Figure 6. Plots of gradient ($|\nabla z|$) and curvature (Laplacian operator, $\nabla^2 z$) for two patches of terrain in the OCR. (A) Relationship of gradient and curvature for steep and dissected terrain (crosses), valley floor (filled gray diamonds), and deep-seated landslides (filled circles). The thick, gray box defines the morphologic signature of deep-seated slides ($0.16 < |\nabla z| < 0.44$ and $|\nabla^2 z| < 0.008$), which is distinct from the signature of other landforms. More than 92% of the deep-seated landslide data points fall within the envelope, whereas only 4%–8% of the data for other landforms are enclosed by the envelope. These estimates are insensitive to the number of data points included for the various landforms. (B) Same as A for an area in the central region of Figure 7. Sporadic steep ($|\nabla z| > 0.44$) points within deep-seated slides are associated with intermittent gully networks and steep slopes near channel margins. Negative curvature is convex upward and positive curvature is concave upward.

slopes north of 44° latitude may reflect greater availability of low-shear-strength siltstone beds, which comprise 40%–50% of the bedrock and frequently exhibit thicknesses greater than 1 m (Heller and Dickinson, 1985). Most generally, these results indicate that landslide-dominated terrain is persistent throughout much of our OCR study area, as up to 25% of the landscape exhibits the topographic signature of deep-seated landsliding (Fig. 8A).

Along our north-south transect, median local relief (estimated using a 2.5 km window) declines progressively (Fig. 8B), coincident with an increase in the incidence of deep-seated landsliding. High-relief terrain in the south (~450 m) gives way to increasingly subtle landforms at the northern extent of the study area, where median relief is ~300 m and exhibits less variability. The progressive decline in relief is locally interrupted between latitudes of 44.1° and 44.5° (see vertical gray band in Fig. 8B), where a cluster of aphanitic, mafic-rich intrusions (see the symbols "I" in Fig. 2A) generates anomalously high local relief. Although we removed topography associated with bedrock other than the Tyee Formation in our analyses, these highly resistant dikes appear to regulate valley incision within Tyee-underlain slopes that flank the intrusions. Adjacent channels are anomalously steep as they connect to headwaters atop the resistant dikes, and small-scale (and thus unmapped) features often form knickpoints and contribute to steepening of channel profiles and elevated values of local relief. Apart from this local departure, relief declines systematically to the north coincident with an increasing frequency of large landslides (Fig. 8).

To further elucidate the influence of deep-seated landsliding on topographic relief, we compared local relief with the fraction of proximal landslide-dominated terrain at 1200 randomly distributed points within the Tyee Formation. At each point, we calculated local relief and the fraction of surrounding terrain with $\beta > 0.33$, F, using windows with radii equal to 250 m and 2.5 km. The median value of hillslope-scale local relief (250 m window) decreases progressively with F (Fig. 9A). Hillslopes largely devoid of large landslides ($F \sim 0$) have median relief values that approach 250 m, whereas median relief for landslide-prone slopes ($F > 0.25$) is consistently lower than 200 m. Our analysis using a 2.5 km window yields slightly different results. First, median values of relief are higher due to the larger sampling area. Second, we observed that where $F < 0.25$, median values of local relief are ~440 m and uniformly exceed 400 m (Fig. 9B). In contrast, where deep-seated landslides comprise more than 25% of the local terrain ($F > 0.25$), median relief is ~340 m, does not exceed 400 m, and exhibits relatively low variability. These results indicate that regional-scale topographic development may be subdued where deep-seated slope failures have altered a sufficient fraction of the terrain. Owing to the absence of systematic variation in additional factors that affect relief (such as rock uplift or ridge/valley spacing), these findings demonstrate that local relief in the OCR is modulated by the pattern of deep-seated landsliding.

STRUCTURAL CONTROLS ON DEEP-SEATED LANDSLIDING

Landsliding in sedimentary units is frequently controlled by bedrock orientation as depositional interfaces exhibit low shear strength that facilitates slope deformation. Considering the series of low-amplitude folds in the Tyee Formation, how does the deformation pattern influence the distribution of deep-seated landslides? One might expect landslide-prone terrain to be pervasive in zones with steeply dipping bedrock. Here, we combine structural data and the distribution of deep-seated slides to explore how bedrock inclination influences the propensity for slope failure.

Method

To test the hypothesis that bedrock structure controls the occurrence of deep-seated slides, we performed a series of analyses combining structural data and our morphology-based mapping of slide-dominated terrain (Fig. 2B). To facilitate the analyses, we digitized 1516 strike and dip measurements from existing geologic maps that coincide with our study area (Baldwin, 1956, 1959, 1961; Wells et al., 2000).

At several locales with high β values (>0.33), we compared the aspect of failure-dominated slopes with the dip and orientation of bedrock. We estimated the aspect of deep-seated landslides as the average downslope direction based on topographic contours (e.g., Fig. 5). If the orientation of Tyee bedding controls landsliding, the aspect of slide-dominated slopes should correspond with bedrock dip direction.

To determine whether the density of slide-prone terrain varies systematically with bedrock inclination, we calculated the distribution of β values within 2.5 km of each strike and dip measurement. If steeper dips increase the probability of deep-seated landsliding, surrounding terrain should exhibit a high proportion of β values that exceed 0.33. We chose to use a 2.5 km window because it enabled us to sample the propensity for landsliding within several ridge/valley sequences around each structural data point. Furthermore, bedrock orientation tends to be relatively consistent over the scale of 2.5 km. Analyses using a larger spatial scale would likely be clouded by variable bedrock geometry.

For each strike and dip measurement, we estimated the fractional of adjacent terrain with β >0.33, *F,* and summarized the resulting data set using 1° bins of bedrock dip. Because landslide-prone terrain is ubiquitous in areas overlying silt-rich distal ramp facies (Fig. 8), bedrock lithology may modulate structural controls on deep-seated landsliding. Specifically, the frequency and thickness of weak siltstone innerbeds may affect the bedrock inclination required to generate instability. To account for this possibility, we separately analyzed terrain north and south of 44° latitude, which serves as an approximate boundary between massive, sand-rich units to the south and thinly bedded silt-rich units to the north.

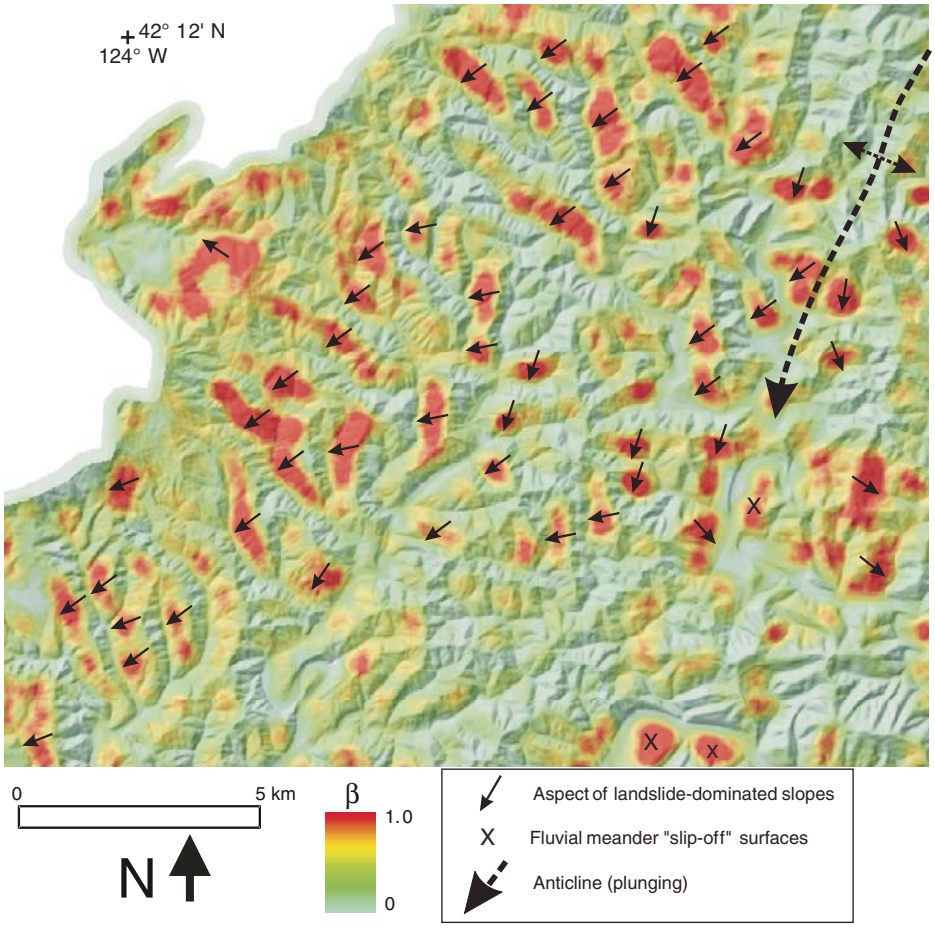

Figure 7. Detailed map of β values for the region shown on Figure 2B (see caption for explanation). Small arrows represent the downhill aspect of slopes with morphology indicative of deep-seated landslides. The northeast-trending anticline (large dashed arrow) indicates the expected direction of bedrock dip angles, which corresponds to the orientation of failure-prone slopes. Symbols demarcate fluvial slip-off surfaces misidentified as deep-seated landslides.

Results

The distribution of landslides in the Tyee Formation is consistent with bedrock orientation. On the western part of the area depicted in Figure 7, landslides are predominantly directed to the southwest, coincident with the bedrock dip associated with the plunging anticline that trends SSE. On the eastern side of the anticline, the aspect of failure-dominated slopes is southeast, confirming the correspondence between dip direction and landslide slope aspect (Fig. 7). Locally, bedrock dip and the downslope aspect of slide-prone slopes exhibit similar orientations (Fig. 10). At the Walton site, the orientation of hillslope failures mirrors bedrock dip directions, which are oriented west and southeast on either side of the plunging fold axis.

In the sand-rich (southern) and silt-rich (northern) regions of our study area, the fraction of landslide-prone terrain, *F*, increases proportionally with bedrock dip angle (Fig. 11). The sensitivity of landsliding to dip angle, however, differs between the two regions. In the southern region, low dip angles are associated with predominantly steep and dissected terrain as the proportion of slide-prone terrain is less than

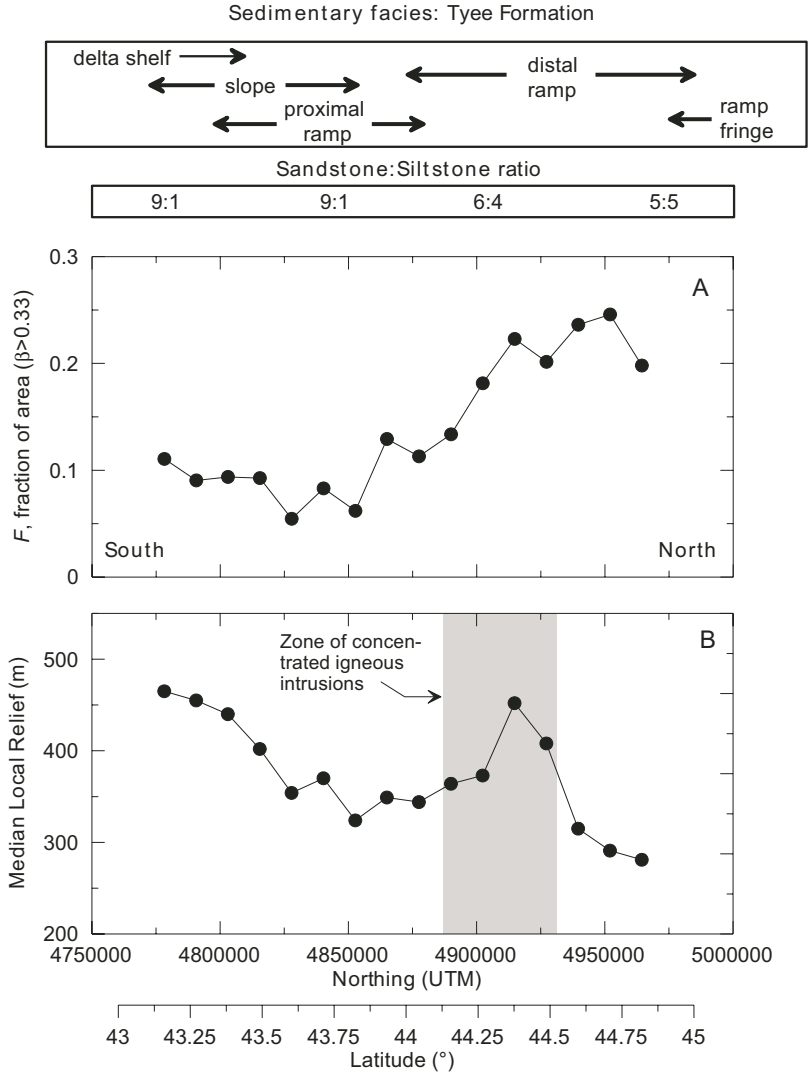

Figure 8. Latitudinal variation in (A) fraction of terrain with β >0.33, and (B) median local relief using a 2.5-km-radius window. Annotations at the top illustrate latitudinal variation in sedimentary facies and the sandstone:siltstone ratio (Chan and Dott, 1983; Heller and Dickinson, 1985). For each plot, data were calculated from sixteen 12.5 km (measured north-south) nonoverlapping swaths. The prevalence of terrain influenced by deep-seated slope instability increases northward, coincident with a decrease in the sandstone:shale ratio and median local relief. The gradual, northward decline in relief is locally perturbed around a zone of concentrated igneous intrusions (see gray box in B). These resistant units generate anomalously high values of relief as they modulate valley incision in adjacent slopes of the Tyee Formation. See Figure 2A for the location of intrusions. UTM refers to Universal Transverse Mercator coordinate system in meters.

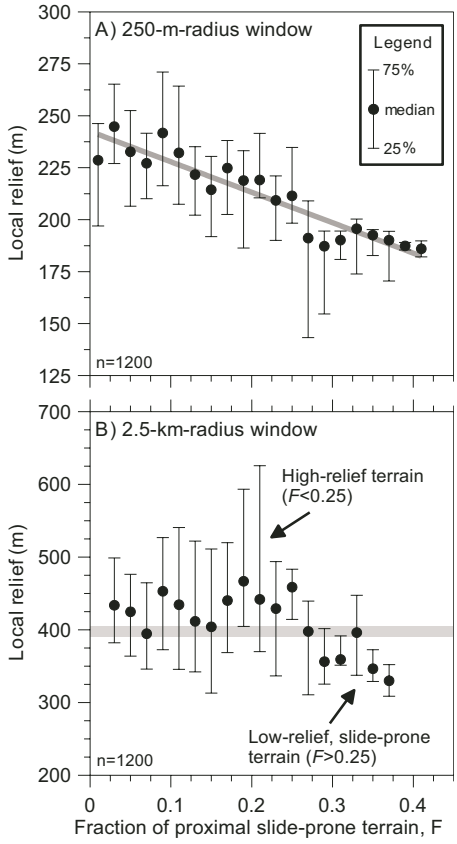

Figure 9. Variation of local relief with the proportion of terrain prone to deep-seated landsliding. At 1200 randomly chosen points within our study area, we used 250-m- and 2.5-km-radius windows to calculate values of local relief and the fraction of adjacent terrain with β >0.33, *F* (see text for description). (A) Median hillslope-scale relief (250 m window) declines linearly with *F*. Summary statistics for the regression line fit to median values: $y = -146.5x + 242.5$, $r^2 = 0.87$. (B) Regional-scale median relief (2.5 km window) is ~440 m, where *F* <0.25 and declines to ~340 m, where *F* >0.25. The thick gray line roughly separates low-relief, slide-prone terrain from high-relief terrain with a smaller density of slope failures. Filled circles and error bars represent the median and upper/lower quartiles for distributions with bin size of 0.02.

2% (Fig. 11A). With increasing bedrock dip, the median value of *F* increases gradually such that 8%–9% of the proximal terrain exhibits the signature of deep-seated sliding where bedrock is inclined 15°–18°. Variability in the proportion of slide-prone terrain (as approximated by the interquartile range) is relatively low, suggesting that bedrock inclination may be the primary control on landsliding. Massive sandstone beds that characterize bedrock in the southern region may require significant inclination before substantial portions of the terrain experience translational deformation. In contrast, our analysis in the northern region indicates that ~10% of the landscape has experienced deep-seated slope instability where the bedrock is nearly horizontal (Fig. 11B). Furthermore, the proportion of slide-prone terrain increases rapidly with dip angle such that nearly 30% of the landscape exhibits the signature of deep-seated landsliding where dip angles approach 15°. For a given dip angle, variability in the fraction of slide-altered terrain is significant, reflecting additional factors that influence the propensity for deep-seated landsliding. The ubiquity of thick siltstone beds in the northern region may modulate both landslide style and thresholds of slope instability.

IMPLICATIONS FOR LANDSCAPE DEVELOPMENT

Continued rock exhumation in the OCR will result in a southward shift of sedimentary facies (Fig. 12). Due to the progradational nature of the Tyee Formation (Heller and Dickinson, 1985), distal and ramp fringe deposits with low sandstone:siltstone ratios will progressively crop out in the central region of our study area as erosion of the OCR proceeds. Owing to the linkage between bedrock lithology, structure, and slope instability, large slope failures will play an increasingly prominent role in shaping the central and eventually southern OCR. The time scale for this process transition can be coarsely estimated using erosion rates (~0.1 mm yr^{-1}) and thickness estimates (2–3 km) of the Tyee Formation. These data indicate that it would take 20–30 m.y. to unroof the entire Tyee Formation. Considering the subsurface architecture of Tyee Formation facies (Heller and Dickinson, 1985), one might expect the current surficial facies distribution to shift 20–40 km southward over 2–3 m.y. Given that uplift in the OCR has been active since the late Miocene (McNeill et al., 2000), the north-to-south replacement of steep/dissected terrain with deep-seated landslides is likely an ongoing process. This conceptual model suggests that landslide-dominated, low-relief terrain will cannibalize steep and dissected topography in the central OCR. As a result, the dominant role of debris flows in sculpting drainage basins will be transferred to episodic, large-magnitude mass movements that frequently dam valleys and punctuate sediment delivery (Fig. 12). Complications to this simplified model include localized aphanitic dikes that limit the incision of adjacent terrain and tend to favor the maintenance of long, high-relief slopes.

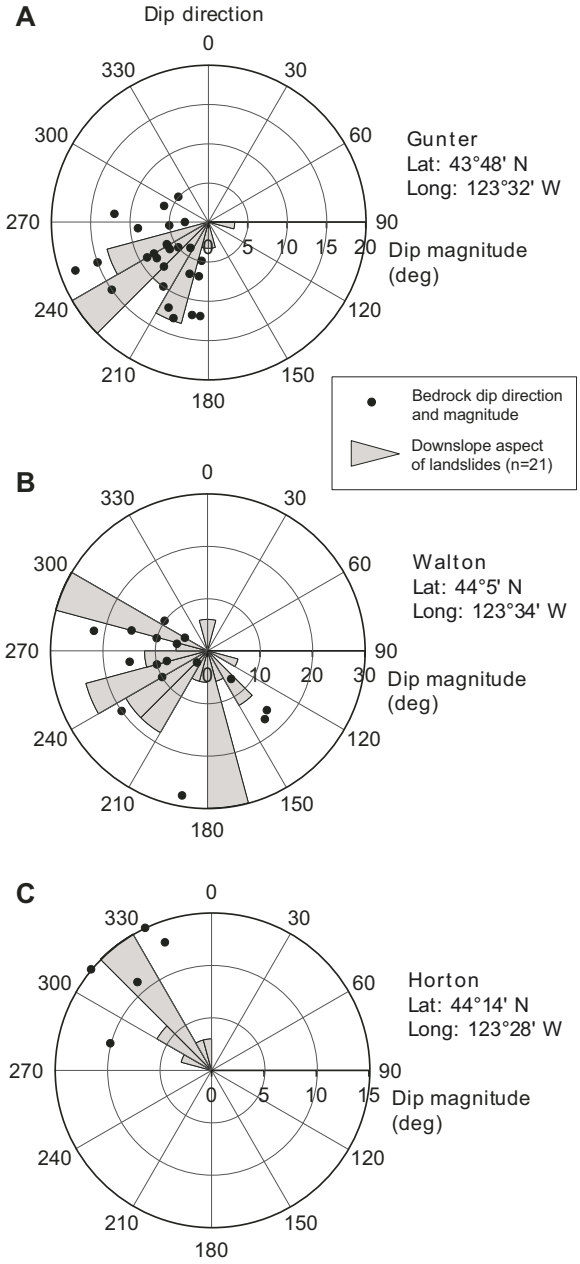

Figure 10. Rose and polar plots illustrating the correspondence between the aspect of failure-prone slopes (gray pie slices) and the dip and direction of bedrock (filled circles) for three regions within our study area. Data collected within the (A) Gunter, (B) Walton, and (C) Horton, U.S. Geological Survey (USGS) 7.5′ 1:24k topographic quadrangles. Distance from the origin represents the magnitude of bedrock dip (filled circles) and the relative frequency of failure-prone slopes with a given aspect (gray pie slices). Hillslope aspect data were binned in 15° intervals.

DISCUSSION

Our results indicate that deep-seated landsliding is pervasive in the OCR and will continue to play a prominent role in shaping the landscape according to systematic variations in bedrock structure and lithology. In a recent study, Montgomery (2001) focused on shallow landslide susceptibility and analyzed slope distributions across a broader expanse of the OCR than analyzed here, suggesting that systematic variations in relief and hillslope gradient primarily reflect variation in tectonic forcing and rock type. In contrast, our analysis emphasizes the role of large, bedrock landslides in regulating topographic development of the OCR underlain by the Tyee Formation. Local relief decreases with the fraction of area altered by deep-seated landsliding and does not appear to reflect variations in rock uplift rate (Kelsey et al., 1996).

The topographic algorithm we employed to derive these insights is not necessarily intended for use in site-specific analyses of landslide potential but instead enables us to identify slopes whose morphology is indicative of deep-seated landsliding. Our methodology performed well in areas where we compared model predictions with field observations; however, we observed several instances where the algorithm misidentified fluvial meander slip-off surfaces as failure-prone slopes. Although this misrepresentation does not affect our conclusions about the relative importance of deep-seated landsliding because such meanders are localized and

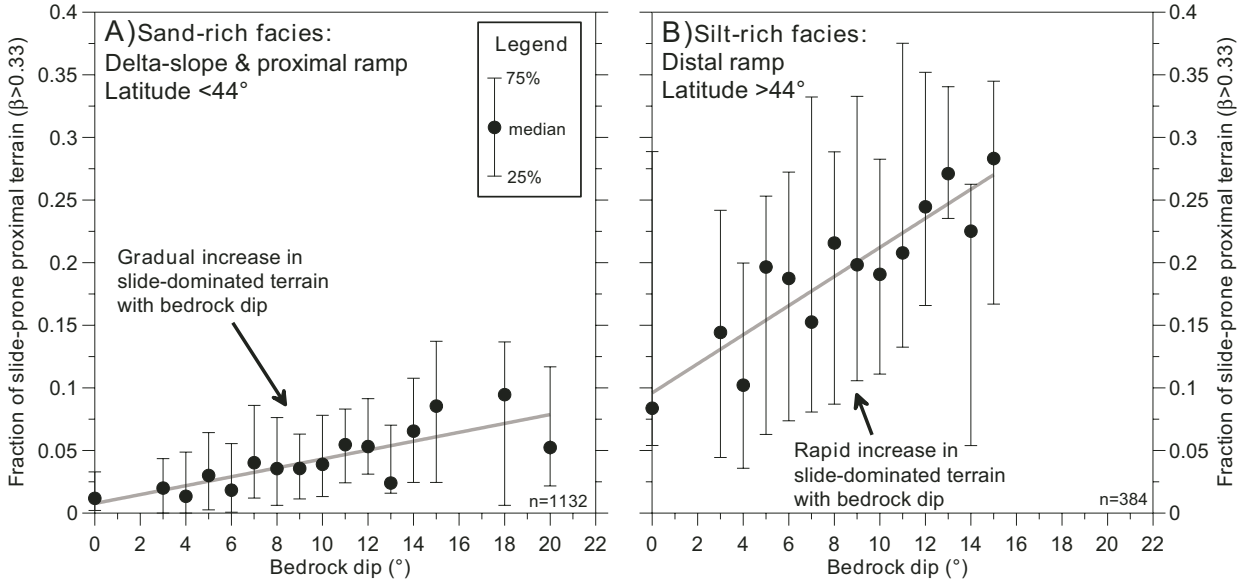

Figure 11. Variation in the fraction of slide-prone terrain with bedrock dip angle for (A) sand-rich facies south of 44° latitude, and (B) silt-rich facies north of 44° latitude. For each strike and dip observation (n = 1516), we calculated the fraction of surrounding terrain (within 2.5 km) with β >0.33. Each data point represents the median value for 1° bins of bedrock dip angle. Upper and lower error bars represent the 75th and 25th percentile values, respectively. The extent of failure-prone terrain increases linearly with dip in both regions, although the silt-rich areas exhibit a higher proportion of landslide-prone terrain for a given bedrock dip angle. Summary statistics for linear regressions fit to the median values are: $y = 0.0035x + 0.0077$, $r^2 = 0.65$ for the sand-rich region and $y = 0.0116x + 0.096$, $r^2 = 0.81$ for the silt-rich region. We did not calculate median values for bins with fewer than 10 data points.

sparse in the OCR, additional morphologic criteria that account for proximity and geometry of nearby valleys are needed.

Calibration of our algorithm depended on the resolution of topographic data. In particular, the grid spacing of DEMs determined the nature of the morphologic signature used to identify landforms. Interestingly, our observation that large landslides are smooth and relatively planar when compared to adjacent stable terrain may be reversed when meter-scale morphologic data are employed. In contrast to our analysis using ~26.5 m data, a recent study that used ~1 m data derived from airborne laser swath mapping (ALSM) indicates that slide-prone terrain is highly roughened and irregular compared to adjacent, unfailed slopes, and that it exhibits varying degrees of roughness depending on the time since instability (McKean and Roering, 2004). Furthermore, the scale of our topographic data and the width of our smoothing window limited the spatial extent of landslide-dominated terrain that could be identified. Although our map of β values accurately located large, ancient slide masses, it less effectively distinguished small segments of hillslopes that experienced deep-seated slide activity. During our field visits, we noted numerous headscarps and benchlike landforms at the scale of ~100 × 100 m that did not consistently generate values of β >0.33. Many of these smaller landslides exhibited somewhat elevated β (0.1–0.3) values and thus were classed in the transitional category (yellow color in Fig. 2B). In contrast to our simple, bivariate method of distinguishing deep-seated landslides, more elegant statistical methods that incorporate principal component analysis have been effectively applied toward a similar end (e.g., Howard, 1995).

The prevalence of landslide-dam lakes in the OCR offers an additional opportunity to test our algorithm. The slopes adjacent to each of the lakes (Table 1) exhibited patches having the morphologic signature of deep-seated landsliding (β >0.33). In particular, the landslide deposit responsible for creating Triangle Lake and the upstream alluviated valley, which exceed 10 km^2 in area, has β >0.33, and the size of the feature is typical for failure-prone slopes in the OCR (~1 km^2). From estimates of typical landslide size and our calculations of landslide density, at least 2000 deep-seated landslides persist in the OCR.

Thick, highly weathered soils, relatively smooth headscarps, and extensive alluvial fills associated with landslides in the OCR suggest that these large slope failures have persisted in the landscape for long periods of time (>10 k.y.). Once initiated, deep-seated failures may episodically occur at a particular location due to the inclination of low-shear-strength siltstone beds and preferential groundwater flow along sedimentary interfaces. Currently, it is unclear whether slopes prone to deep-seated activity can be recolonized by the processes that shape steep and dissected terrain (i.e., fluvial and debris flow incision). We observed sparse evidence of large, contiguous failure-prone slopes experiencing renewed dissection. This may indicate that deep-seated landslides remain sufficiently active to subvert valley dissection and steepening. The conditions for valley-forming processes (such as shallow landsliding and erosion associated with overland flow and seepage) on the low-gradient and low-drainage area slopes of large landslides are unfavorable according to slope-drainage area channelization thresholds (Montgomery and Dietrich, 1988). Most generally, terrain in the OCR appears to be largely bimodal, as it is characterized by steep, debris-flow–prone ridge and valley sequences and by gentle, benchlike deep-seated landslides.

The timing and triggering mechanisms of large slides in the Tyee Formation are uncertain. The few examples of historically active deep-seated slides have occurred on slopes whose morphology suggests previous alteration by deep-seated slope instability (Thrall et al., 1980). In some cases, minor movement of deep-seated landslides appears to have initiated due to loading effects of road waste deposition

(Seward and Blackwood, 1998). Historical rainfall events have occasionally been sufficient to reactivate older slides, but the relative importance of valley incision, hydrologic events, or seismic activity in initiating new failures remains to be explored. The location of the OCR above an active subduction zone suggests that infrequent, large-magnitude earthquakes (Atwater et al., 1991; Nelson et al., 1995) may have contributed to landslide initiation, but the lack of historical observations makes this hypothesis difficult to test. Coseismic landslides of similar scale have been documented for recent seismic events (King et al., 1987; Martinez et al., 1995; Schuster et al., 1998; Guzzetti et al., 2002; Khazai et al., 2004). Establishment of a high-resolution landslide chronology record via lake cores or internal slump ponds may reveal the synchronicity of failure events. The two available dates for the formation of landslide-dam lakes in our study area (1.4 ka for Loon Lake and >40 ka for Triangle Lake) are disparate and the degree to which deep-seated activity has persisted through the Late Quaternary evolution of the OCR remains to be shown.

The correspondence between bedrock structure, lithology, and hillslope aspect provides local control on deep-seated landsliding in the Tyee Formation and other regions (e.g., Schmidt and Montgomery, 1996; Jackson, 2002) and may drive variability in the frequency of deep-seated landslide terrain estimated around the strike and dip measurements (Fig. 11). In the northern section of our study area, distributions of β values indicate that aspects of failure-prone slopes are locally less uniform than observed elsewhere. The high density of slide-dominated terrain in the northern section of our study area suggests that the mechanical requirement that dip slopes correspond with hillslope aspect may be relaxed. Here, the predominance of thick, low-strength siltstone beds may facilitate slope failures over a broader range of slope geometries. The style of slope failure also appears to vary across our study area as large translational slope failures dominate in the southern region, and rotational slips are more common in the northern region.

Our conceptual model that forecasts a north-to-south, landslide-driven unzippering of relief in the OCR is derived through a synthesis of topographic, structural, and lithologic data. Additional factors that may affect our relief calculations include variable rates of base-level lowering and the positioning of major and minor river systems. Terrain at the southern tip of our study area exhibits high values of relief that may be affected by differential uplift rates to the south and associated drainage basin adjustment.

In many active tectonic areas underlain by fine-grained sedimentary bedrock (e.g., Eel River, northern California; upper Waipaoa River, New Zealand; and the Eastern Coast Range, Taiwan), patterns of sediment production are dominated by large landslides, and local relief is low (~300–400 m) despite rapid rates of rock uplift (~1–5 mm yr^{-1}). In such areas, the frequency and magnitude of slope failure may be sufficient to prevent the development of relief typically associated with high uplift regions. Although rates of tectonic forcing in the OCR are low in comparison, large landslides likely temper the coupling between tectonic forcing and local relief because they affect the entire hillslope and impose low gradients over broad areas.

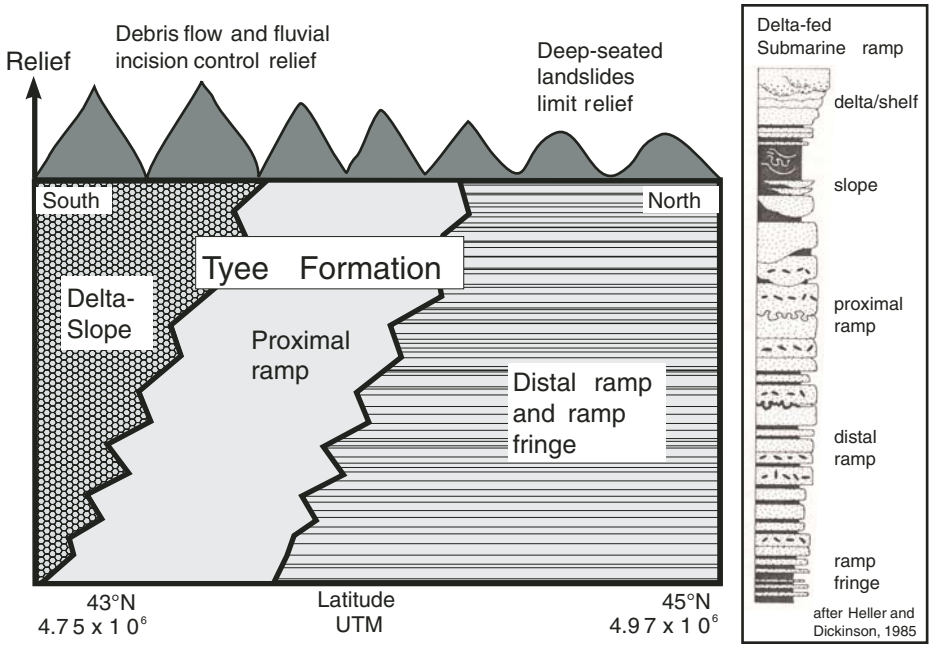

Figure 12. Schematic illustration of the topographic manifestation of sedimentary facies of the Tyee Formation. Silt-rich distal and ramp fringe deposits in the north tend to generate large, deep-seated landslides and low-relief terrain. Sand-rich deltaic facies in the south are predominantly characterized by high relief terrain with relatively low rates of slope alteration by large, bedrock landslides. Continued exhumation of the Tyee Formation will result in a southward shift of slide-prone, low-relief terrain underlain by silt-rich distal facies. UTM refers to Universal Transverse Mercator coordinate system in meters.

CONCLUSION

In contrast to the steep and dissected, debris-flow–prone terrain often cited as characteristic of the Oregon Coast Range, terrain prone to deep-seated landsliding is pervasive and exhibits low-gradient, benchlike morphologies. We defined the topographic signature of deep-seated landslides and developed an automated algorithm to map the extent of terrain altered by slope failure. The particular algorithm we employed was developed specifically for slopes in the OCR; however, the general approach described here may be applicable for mapping and identifying large landslides in other landscapes. The fraction of terrain affected by deep-seated landsliding varies from 5%–25% as a function of bedrock structure and lithologic variations. The frequency and thickness of low-shear-strength siltstone beds in the sand-rich deltaic-turbidite deposits of the Tyee Formation increase to the north, coincident with a systematic increase in the fraction of terrain dominated by deep-seated landsliding.

The fraction of slide-prone terrain increases proportionally with bedrock dip angle and in the northern region of our study area, where nearly 30% of the landscapes exhibit the signature of deep-seated landsliding. Local relief declines correspondingly, implying that deep-seated landsliding imparts a first-order control on landscape development. Our analyses suggest that continued exhumation in the OCR will result in a southward shift of distal silt-rich facies, enabling us to generate quantitative predictions for the evolution of the OCR. The progressive emergence of the slide-prone units should drive a north-to-south decline in relief over million-year time scales. Our findings are consistent with recent hypotheses that large landslides can effectively decouple relief development from tectonic

forcing and emphasize the importance of considering stratigraphic and structural data when analyzing how surface processes shape mountainous landscapes. In the OCR, structural and lithologic controls are responsible for systematic variations in the distribution of landslides and imply that there is no single universal limit to topographic development. Large landslides in the OCR are pervasive and long-lived, suggesting that they may serve as important controls on the evolution and distribution of salmonids, whose biology is strongly linked with natural disturbances in the Pacific Northwest. Because large landslides in the region may reflect large-magnitude earthquakes associated with the Cascadia subduction zone, the method developed here may aid in the assessment of geologic hazards and land management practices.

ACKNOWLEDGMENTS

The first author thanks the Department of Geological Sciences, University of Oregon, for financial support. Kate van Ourkerk (UO) and Craig Stephens (UO) accurately digitized structural data and Barry Williams (BLM) provided logistical field support early in the study. Jim McKean (USFS) offered helpful comments on an early draft. Review comments by David Harbor, Lionel Jackson, and an anonymous reviewer significantly improved this contribution. The authors are particularly indebted to Associate Editor Jon Major for his careful and thoughtful review.

REFERENCES CITED

Ahnert, F., 1970, Functional relationships between denudation, relief and uplift in large, mid-latitude drainage basins: American Journal of Science, v. 268, p. 243–263.

Ahnert, F., 1984, Local relief and the height limits of mountain ranges: American Journal of Science, v. 284, no. 9, p. 1035–1055.

Atwater, B.F., Stuiver, M., and Yamaguchi, D.K., 1991, Radiocarbon test of earthquake magnitude at the Cascadia subduction zone: Nature, v. 353, no. 6340, p. 156–158, doi: 10.1038/353156a0.

Baldwin, E.M., 1956, Geologic map of the lower Siuslaw River area, Oregon: U.S. Geological Survey Oil and Gas Investigations Map OM-186, scale 1:62,500.

Baldwin, E.M., 1958, Landslide lakes in the Coast Range of Oregon: Geological Newsletter, Geological Society of the Oregon Country, v. 24, no. 4, p. 23–24.

Baldwin, E.M., 1959, Geology of the Marys Peak and Alsea quadrangles, Oregon: U.S. Geological Survey, Oil and Gas Investigations Map OM-0162, scale 1:62,500.

Baldwin, E.M., 1961, Geologic map of the lower Umpqua River area, Oregon: U.S. Geological Survey, Oil and Gas Investigations Map, OM-0204, scale 1:62,500.

Benda, L.E., 1990, The influence of debris flows on channels and valley floors in the Oregon Coast Range, USA: Earth Surface Processes and Landforms, v. 15, p. 457–466.

Benda, L., and Dunne, T., 1997, Stochastic forcing of sediment supply to channel networks from landsliding and debris flow: Water Resources Research, v. 33, no. 12, p. 2849–2863, doi: 10.1029/97WR02388.

Beschta, R.L., 1978, Long-term patterns of sediment production following road construction and logging in the Oregon Coast Range: Water Resources Research, v. 14, p. 1011–1016.

Brocklehurst, S.H., and Whipple, K.X, 2002, Glacial erosion and relief production in the Eastern Sierra Nevada, California: Geomorphology, v. 42, no. 1-2, p. 1–24, doi: 10.1016/S0169-555X(01)00069-1.

Carson, M.A., and Petley, D.J., 1970, The existence of threshold hillslopes in the denudation of the landscape: Transactions (Institute of British Geographers: 1965), v. 49, p. 71–95.

Cendrero, A., and Dramis, F., 1993, The contribution of landslides to landscape evolution in Europe: Geomorphology, v. 15, no. 3-4, p. 191–211, doi: 10.1016/0169-555X(95)00070-L.

Chan, M.A., and Dott, J., R.H., 1983, Shelf and deep-sea sedimentation in Eocene forearc basin, Western Oregon—Fan or non-fan?: American Association of Petroleum Geologists Bulletin, v. 67, p. 2100–2116.

Chan, M.A., and Dott, R.H., Jr., 1986, Depositional facies and progradational sequences in Eocene wave-dominated deltaic complexes, southwestern Oregon: American Association of Petroleum Geologists Bulletin, v. 70, no. 4, p. 415–429.

de la Fuente, J., Elder, D., and Miller, A., 2002, Does deforestation influence the activity of deep-seated landslides? Observations from the flood of 1997 in the Central Klamath Mountains, Northern California: Geological Society of America, Abstracts with Programs, v. 34, no. 5, p. 88.

Densmore, A.L., and Hovius, N., 2000, Topographic fingerprints of bedrock landslides: Geology, v. 28, p. 371–374, doi: 10.1130/0091-7613(2000)0282.3.CO;2.

Densmore, A.L., Ellis, M.A., and Anderson, R.S., 1998, Landsliding and the evolution of normal-fault-bounded mountains: Journal of Geophysical Research, v. 103, no. B7, p. 15,203–15,219, doi: 10.1029/98JB00510.

Dietrich, W.E., and Dunne, T., 1978, Sediment budget for a small catchment in mountainous terrain: Zeitschrift fur Geomorphologie, Supplement, v. 29, p. 191–206.

Dietrich, W.E., Dunne, T., Humphrey, N.F., and Reid, L.M., 1982, Construction of sediment budgets for drainage basins, *in* Swanson, F.J.J., Journal, R., Dunne, T., Swanston, D.N., eds., Sediment Budgets and Routing in Forested Drainage Basins: U.S. Department of Agriculture, p. 5–23.

Dikau, R., and Schrott, L., 1999, The temporal stability and activity of landslides in Europe with respect to climatic change (TESLEC): Main objectives and results: Geomorphology, v. 30, p. 1–12, doi: 10.1016/S0169-555X(99)00040-9.

Gabet, E.J., Pratt-Sitaula, B.A., and Burbank, D., 2004, Climatic controls on hillslope angle and relief in the Himalayas: Geology, v. 32, p. 629–632, doi: 10.1130/G20641.1.

Gerstel, W.J., and Badger, T.C., 2002, Hydrologic controls and forest land management implications for deep-seated landslides; examples from the Lincoln Creek Formation, Washington: Geological Society of America, Abstracts with Programs, v. 34, no. 5, p. 89.

Gonzalez-Diez, A., Remondo, J., de Teran, J.R.D., and Cendrero, A., 1999, A methodological approach for the analysis of the temporal occurrence and triggering factors of landslides: Geomorphology, v. 30, no. 1-2, p. 95–113, doi: 10.1016/S0169-555X(99)00047-1.

Guzzetti, F., Malamud, B.D., Turcotte, D.L., and Reichenbach, P., 2002, Power-law correlations of landslide areas in central Italy: Earth and Planetary Science Letters, v. 195, no. 3-4, p. 169–183, doi: 10.1016/S0012-821X(01)00589-1.

Harp, E.L., and Jibson, R.W., 1996, Landslides triggered by the 1994 Northridge, California, earthquake: Bulletin of the Seismological Society of America, v. 86, p. 319–332.

Heimsath, A.M., Dietrich, W.E., Nishiizumi, K., and Finkel, R.C., 2001, Stochastic processes of soil production and transport: Erosion rates, topographic variation and cosmogenic nuclides in the Oregon Coast Range: Earth Surface Processes and Landforms, v. 26, no. 5, p. 531–552, doi: 10.1002/esp.209.

Heller, P.L., and Dickinson, W.R., 1985, Submarine ramp facies model for delta-fed, sand-rich turbidite systems: American Association of Petroleum Geologists Bulletin, v. 69, no. 6, p. 960–976.

Heller, P.L., and Ryberg, P.T., 1983, Sedimentary record of subduction to forearc transition in the rotated Eocene basin of western Oregon: Geology, v. 11, p. 380–383.

Hermanns, R.L., and Strecker, M.R., 1999, Structural and lithological controls on large Quaternary rock avalanches (sturzstroms) in arid northwestern Argentina: Geological Society of America Bulletin, v. 111, p. 934–948, doi: 10.1130/0016-7606(1999)1112.3.CO;2.

Hermanns, R.L., Trauth, M.H., Niedermann, S., McWilliams, M., and Strecker, M.R., 2000, Tephrochronologic constraints on temporal distribution of large landslides in northwest Argentina: Journal of Geology, v. 108, no. 1, p. 35–52, doi: 10.1086/314383.

Hooke, R.L., 2003, Time constant for equilibration of erosion with tectonic uplift: Geology, v. 31, p. 621–624, doi: 10.1130/0091-7613(2003)0312.0.CO;2.

Hovius, N., Stark, C.P., and Allen, P.A., 1997, Sediment flux from a mountain belt derived by landslide mapping: Geology, v. 25, p. 231–234, doi: 10.1130/0091-7613(1997)0252.3.CO;2.

Hovius, N., Stark, C.P., Tutton, M.A., and Abbott, L.D., 1998, Landslide-driven drainage network evolution in a pre-steady-state mountain belt: Finisterre Mountains, Papua New Guinea: Geology, v. 26, p. 1071–1074, doi: 10.1130/0091-7613(1998)0262.3.CO;2.

Hovius, N., Stark, C.P., Chu, H.T., and Lin, J.C., 2000, Supply and removal of sediment in a landslide-dominated mountain belt: Central Range, Taiwan: Journal of Geology, v. 108, no. 1, p. 73–89, doi: 10.1086/314387.

Howard, A.D., 1995, Simulation modeling and statistical classification of escarpment planforms: Geomorphology, v. 12, no. 3, p. 187–214, doi: 10.1016/0169-555X(95)00004-O.

Hurtrez, J.-E., Lucazeau, F., Lave, J., and Avouac, J.-P., 1999, Investigation of the relationships between basin morphology, tectonic uplift, and denudation from the study of an active fold belt in the Siwalik Hills, central Nepal: Journal of Geophysical Research, v. 104, p. 12,779–12,796, doi: 10.1029/1998JB900098.

Jackson, L.E., 2002, Landslides and landscape evolution in the Rocky Mountains and adjacent Foothills area, southwestern Alberta, Canada: Reviews in Engineering Geology, v. 15, p. 325–344.

Kelsey, H.M., 1988, Formation of inner gorges: Catena, v. 15, no. 5, p. 433–458, doi: 10.1016/0341-8162(88)90063-X.

Kelsey, H.M., Ticknor, R.L., Bockheim, J.G., and Mitchell, C.E., 1996, Quaternary upper plate deformation in coastal Oregon: Geological Society of America Bulletin, v. 108, p. 843–860, doi: 10.1130/0016-7606(1996)1082.3.CO;2.

Khazai, B., Sitar, N., and Juang, C.H., 2004, Evaluation of factors controlling earthquake-induced landslides caused by Chi-chi earthquake and comparison with the Northridge and Loma Prieta events: Engineering Geology, v. 71, no. 1-2, p. 79–95, doi: 10.1016/S0013-7952(03)00127-3.

King, J.P., Loveday, I.C., and Schuster, R.L., 1987, Failure of a massive earthquake-induced landslide dam in Papua New Guinea: Earthquakes and Volcanoes, v. 19, no. 2, p. 40–47.

Kuhni, A., and Pfiffner, O.A., 2001, The relief of the Swiss Alps and adjacent areas and its relation to lithology and structure: Topographic analysis from a 250-m DEM: Geomorphology, v. 41, no. 4, p. 285–307, doi: 10.1016/S0169-555X(01)00060-5.

Lague, D., and Davy, P., 2003, Constraints on the long-term colluvial erosion law by analyzing slope-area relationships at various tectonic uplift rates in the Siwaliks Hills (Nepal): Journal of Geophysical Research—Solid Earth, v. 108, no. B2, 2129.

Lancaster, S.T., and Hayes, S.K., 2003, Effects of wood on debris flow runout in small mountain watersheds: American Geophysical Union, Water Resources Research, v. 39, no. 6, 1168.

Lane, J.W., 1987, Relations between geology and mass movement features in a part of the East Fork Coquille River Watershed, Southern Coast Range, Oregon [M.S. thesis]: Corvallis, Oregon State University, 107 p.

Larsen, M.C., and Torres-Sanchez, A.J., 1998, The frequency and distribution of recent landslides in three montane tropical regions of Puerto Rico: Geomorphology, v. 24, no. 4, p. 309–331, doi: 10.1016/S0169-555X(98)00023-3.

Lovell, J.P.B., 1969, Tyee Formation: Undeformed turbidites and their lateral equivalents: Mineralogy and paleogeography: Geological Society of America Bulletin, v. 80, p. 9–22.

Malamud, B.D., Turcotte, D.L., Guzzetti, F., and Reichenbach, P., 2004, Landslide inventories and their statistical properties: Earth Surface Processes and Landforms, v. 29, no. 6, p. 687–711, doi: 10.1002/esp.1064.

Martinez, J.M., Avila, G., Agudelo, A., Schuster, R.L., Casadevall, T.J., and Scott, K.M., 1995, Landslides and debris flows triggered by the 6 June 1994 Paez earthquake, southwestern Colombia: Landslide News, v. 9, p. 13–15.

Mather, A.E., Griffiths, J.S., and Stokes, M., 2003, Anatomy of a 'fossil' landslide from the Pleistocene of SE Spain: Geomorphology, v. 50, no. 1-3, p. 135–149, doi: 10.1016/S0169-555X(02)00211-8.

May, C.L., 2002, Debris flows through different forest age classes in the central Oregon Coast Range: Journal of the American Water Resources Association, v. 38, no. 4, p. 1097–1113.

May, C.L., and Gresswell, R.E., 2003, Processes and rates of sediment and wood accumulation in headwater streams of the Oregon Coast Range, USA: Earth Surface Processes and Landforms, v. 28, no. 4, p. 409–424, doi: 10.1002/esp.450.

McKean, J.A., and Roering, J.J., 2004, Landslide detection and surface morphology mapping with airborne laser altimetry: Geomorphology, v. 57, p. 331–351, doi: 10.1016/S0169-555X(03)00164-8.

McNeill, L.C., Goldfinger, C., Kulm, L.D., and Yeats, R.S., 2000, Tectonics of the Neogene Cascadia forearc basin: Investigations of a deformed late Miocene unconformity: Geological Society of America Bulletin, v. 112, p. 1209–1224, doi: 10.1130/0016-7606(2000)1122.3.CO;2.

Miller, D.J., and Sias, J., 1998, Deciphering large landslides: Linking hydrological, groundwater and slope stability models through GIS: Hydrological Processes, v. 12, p. 923–941, doi: 10.1002/(SICI)1099-1085(199805)12:63.0.CO;2-3.

Mitchell, C.E., Vincent, P., Weldon, R.J., and Richards, M., 1994, Present-day vertical deformation of the Cascadia margin, Pacific Northwest, United States: Journal of Geophysical Research, v. 99, p. 12,257–12,277, doi: 10.1029/94JB00279.

Molnar, P., and England, P.C., 1990, Late Cenozoic uplift of mountain ranges and global climate change; chicken or egg?: Nature, v. 346, no. 6279, p. 29–34, doi: 10.1038/346029a0.

Montgomery, D.R., 2001, Slope distributions, threshold hillslopes, and steady-state topography: American Journal of Science, v. 301, no. 4-5, p. 432–454.

Montgomery, D.R., and Brandon, M.T., 2002, Topographic controls on erosion rates in tectonically active mountain ranges: Earth and Planetary Science Letters, v. 201, p. 481–489, doi: 10.1016/S0012-821X(02)00725-2.

Montgomery, D.R., and Dietrich, W.E., 1988, Where do channels begin?: Nature, v. 336, no. 6196, p. 232–234, doi: 10.1038/336232a0.

Montgomery, D.R., and Dietrich, W.E., 1994, A physically based model for the topographic control on shallow landsliding: Water Resources Research, v. 30, no. 4, p. 1153–1171, doi: 10.1029/93WR02979.

Montgomery, D.R., Schmidt, K.M., Dietrich, W.E., and Greenberg, H., 2000, Forest clearing and reigonal landsliding: Geology, v. 28, p. 311–314, doi: 10.1130/0091-7613(2000)0282.3.CO;2.

Montgomery, D.R., Balco, G., and Willett, S.D., 2001, Climate, tectonics, and the morphology of the Andes: Geology, v. 29, p. 579–582, doi: 10.1130/0091-7613(2001)0292.0.CO;2.

Moore, I.D., Grayson, R.D., and Ladson, A.R., 1991, Digital terrain modelling; a review of hydrological, geomorphological and biological applications: Hydrological Processes, v. 5, no. 1, p. 3–30.

Mutti, E., and Ricci-Lucchi, F., 1978, Turbidites of the northern Apennines: Introduction to facies analysis: International Geology Review, v. 20, p. 125–166.

Nelson, A.R., Atwater, B.F., Bobrowsky, P.T., Bradley, L.-A., Clague, J.J., Carver, G.A., Darienzo, M.E., Grant, W.C., Krueger, H.W., Sparks, R.J., Stafford, T.W., and Stuiver, M., 1995, Radiocarbon evidence for extensive plate-boundary rupture about 300 years ago at the Cascadia subduction zone: Nature, v. 378, no. 6555, p. 371–374, doi: 10.1038/378371a0.

Ohmori, H., 1993, Changes in the hypsometric curve through mountain building resulting from concurrent tectonics and denudation: Geomorphology, v. 8, no. 4, p. 263–277, doi: 10.1016/0169-555X(93)90023-U.

Orr, E.L., Orr, W.N., and Baldwin, E.M., 1992, Geology of Oregon: Dubuque, Kendall/Hunt, 254 p.

Palmquist, R.C., and Bible, G., 1980, Conceptual modelling of landslide distribution in time and space: Bulletin of the International Association of Engineering Geology, v. 21, p. 178–186.

Personius, S.F., 1995, Late Quaternary stream incision and uplift in the forearc of the Cascadia subduction zone, western Oregon: Journal of Geophysical Research, v. 100, p. 20,193–20,210, doi: 10.1029/95JB01684.

Pinet, P., and Souriau, M., 1988, Continental erosion and large-scale relief: Tectonics, v. 7, p. 563–582.

Pratt, B., Burbank, D.W., Heimsath, A., and Ojha, T., 2002, Impulsive alluviation during early Holocene strengthened monsoons, central Nepal Himalaya: Geology, v. 30, p. 911–914, doi: 10.1130/0091-7613(2002)0302.0.CO;2.

Reneau, S.L., and Dietrich, W.E., 1990, Depositional history of hollows on steep hillslopes, coastal Oregon and Washington: National Geographic Research, v. 6, no. 2, p. 220–230.

Reneau, S.L., and Dietrich, W.E., 1991, Erosion rates in the Southern Oregon Coast Range: Evidence for an equilibrium between hillslope erosion and sediment yield: Earth Surface Processes and Landforms, v. 16, no. 4, p. 307–322.

Roe, G.H., Montgomery, D.R., and Hallet, B., 2003, Orographic precipitation and the relief of mountain ranges: Journal of Geophysical Research—Solid Earth, v. 108, no. B6, 2315.

Roering, J.J., Kirchner, J.W., and Dietrich, W.E., 1996, Identification and characterization of deep-seated landslides in the Oregon Coast Range using digital terrain data: Eos (Transactions American Geophysical Union), v. 77, p. 246.

Roering, J.J., Kirchner, J.W., and Dietrich, W.E., 1999, Evidence for nonlinear, diffusive sediment transport on hillslopes and implications for landscape morphology: Water Resources Research, v. 35, no. 3, p. 853–870, doi: 10.1029/1998WR900090.

Roering, J.J., Kirchner, J.W., and Dietrich, W.E., 2001, Hillslope evolution by nonlinear, slope-dependent transport: Steady-state morphology and equilibrium adjustment timescales: Journal of Geophysical Research, v. 106, no. B8, p. 16,499–16,513, doi: 10.1029/2001JB000323.

Schmidt, K.M., and Montgomery, D.R., 1995, Limits to relief: Science, v. 270, p. 617–620.

Schmidt, K.M., and Montgomery, D.R., 1996, Rock mass strength assessment for bedrock landsliding: Environmental & Engineering Geoscience, v. 2, no. 3, p. 325–338.

Schmidt, K.M., Roering, J.J., Stock, J.D., Dietrich, W.E., Montgomery, D.R., and Schaub, T., 2001, The variability of root cohesion as an influence on shallow landslide susceptibility in the Oregon Coast Range: Canadian Geotechnical Journal, v. 38, p. 995–1024, doi: 10.1139/cgj-38-5-995.

Schuster, R.L., 1978, Landslides: Analysis and Control: Washington, D.C. National Research Council, Transportation Research Board Special Report 176, p. 1–10.

Schuster, R.L., Wieczorek, G.F., Hope, D.G., II, and Keefer, D.K., 1998, Landslide dams in Santa Cruz County, California, resulting from the earthquake: U.S. Geological Survey Professional Paper 1551-C, p. C51–C70.

Seidl, M.A., and Dietrich, W.E., 1992, The problem of channel erosion into bedrock: Catena Supplement, v. 23, p. 101–124.

Seward, J.H., and Blackwood, T., 1998, Loading-induced slope failures on bedding planes in sedimentary geology of the central Oregon Coast Range, *in* Burns, S., ed., Environmental, Groundwater and Engineering Geology: Applications from Oregon: Belmont, California, Star, p. 497–506.

Shroder, J.F., 1998, Slope failure and denudation in the western Himalaya: Geomorphology, v. 26, no. 1-3, p. 81–105, doi: 10.1016/S0169-555X(98)00052-X.

Sklar, L., and Dietrich, W.E., 1999, River longitudinal profiles and bedrock incision models: Stream power and the influence of sediment supply, *in* Tinkler, K., and Wohl, E., eds., Rivers Over Rock: Fluvial Processes in Bedrock Channels: Geophysical Monograph: Washington, D.C., AGU, p. 237–260.

Stark, C.P., and Hovius, N., 2001, The characterization of landslide size distributions: Geophysical Research Letters, v. 28, no. 6, p. 1091–1094, doi: 10.1029/2000GL008527.

Stock, J., and Dietrich, W.E., 2003, Valley incision by debris flows: Evidence of a topographic signature: Water Resources Research, v. 39, no. 4, 1089.

Summerfield, M.A., and Nulton, N.J., 1994, Natural controls of fluvial denudation rates in major world drainage basin: Journal of Geophysical Research, v. 99, no. B7, p. 13,871–13,883, doi: 10.1029/94JB00715.

Thrall, G.F., Jack, R., Johnson, J.J., and Stanley, D.A., 1980, Failure mechanisms of the Drift Creek Slide: Geological Society of America, Abstracts with Programs, v. 12, no. 3, p. 156.

Trauth, M.H., and Strecker, M.R., 1999, Formation of landslide-dammed lakes during a wet period between 40,000 and 25,000 yr BP in northwestern Argentina: Palaeogeography, Palaeoclimatology, Palaeoecology, v. 153, no. 1-4, p. 277–287, doi: 10.1016/S0031-0182(99)00078-4.

Trauth, M.H., Alonso, R.A., Haselton, K.R., Hermanns, R.L., and Strecker, M.R., 2000, Climate change and mass movements in the NW Argentine Andes: Earth and Planetary Science Letters, v. 179, no. 2, p. 243–256, doi: 10.1016/S0012-821X(00)00127-8.

van Asch, T.W.J., and van Steijn, H., 1991, Temporal patterns of mass movements in the French Alps: Catena, v. 18, p. 515–527, doi: 10.1016/0341-8162(91)90052-Y.

Voight, B., 1978, Rockslides and Avalanches, Developments in Geotechnical Engineering: Amsterdam, Elsevier, p. 833.

Walker, G.W., and MacLeod, N.S., 1991, Geologic map of Oregon: U.S. Geological Survey, scale 1:500,000.

Wells, R.E., Jayko, A.S., Niem, A.R., Black, G., Wiley, T., Baldwin, E.M., Molenaar, C.M., Wheeler, K.L., DuRoss, C.B., and Givler, R.W., 2000, Geologic map and database of the Roseburg, Oregon 30' × 60' Quadrangle Douglas and Coos Counties, Oregon: U.S. Geological Survey Open File Report 00-376, scale 1:100,000.

Whipple, K.X, Kirby, E., and Brocklehurst, S.H., 1999, Geomorphic limits to climate-induced increases in topographic relief: Nature, v. 401, p. 39–43, doi: 10.1038/43375.

Wieczorek, G.F., 1984, Preparing a detailed landslide-inventory map for hazard evaluation and reduction: Bulletin of the Association of Engineering Geologists, v. 21, no. 3, p. 337–342.

Willett, S.D., Slingerland, R., and Hovius, N., 2001, Uplift, shortening, and steady-state topography in active mountain belts: American Journal of Science, v. 301, no. 4-5, p. 455–485.

Wong, B.B.-L., 1991, Controls on movement of selected landslides in the Coast Range and western Cascades, Oregon [M.S. thesis]: Corvallis, Oregon State University, 193 p.

Worona, M., and Whitlock, C., 1995, Late Quaternary vegetation and climate history near Little Lake, central Coast Range, Oregon: Geological Society of America Bulletin, v. 107, p. 867–876, doi: 10.1130/0016-7606(1995)1072.3.CO;2.

Zevenbergen, L.W., and Thorne, C.R., 1987, Quantitative analysis of land surface topography: Earth Surface Processes and Landforms, v. 12, p. 47–56.

Zhang, P.Z., Molnar, P., and Downs, W.R., 2001, Increased sedimentation rates and grain sizes 2–4 Myr ago due to the influence of climate change on erosion rates: Nature, v. 410, no. 6831, p. 891–897, doi: 10.1038/35073504.

Manuscript Received by the Society 18 January 2004
Revised Manuscript Received 13 September 2004
Manuscript Accepted 5 October 2004

Printed in the USA